RELABEN Deliverable 1 & Deliverable 2

Stress relaxation of bentonite at high temperatures (RELABEN)

Deliverable 1: INITIAL STATE-OF-THE-ART ON BENTONITE RHEOLOGICAL BEHAVIOUR

Deliverable 2: DETAILED RESEARCH PLAN

Authors	Chang Seok, K., Eriksson, P., Hausmannová, L., Howett, E., Keech, P., Kirby, M., Mašín, D., Najser, J., Niskanen, M., Sellin, P.
Date	12/22/2025
Version	Version 1
Reference	2025/Report/RELABEN-D1D2

Document Revision History		
Version	**Date**	**Summary**
Version 1	12/22/2025	

12/22/2025

IGD-TP c/o National Cooperative for the Disposal of Radioactive Waste (Nagra),
Hardstrasse 73, CH-5430 Wettingen
Tel. +41 56 437 11 11, www.nagra.ch, info@nagra.ch

Contents

1 Introduction 4

2 Initial state-of-the-art on bentonite rheological behaviour 5

2.1 Charles University (SURAO) 5

2.1.1 BCV bentonite 5

2.1.2 Experimental equipment 5

2.1.3 Testing programme 7

2.1.4 Results 8

2.2 SKB 18

Freezing of bentonite 18

Observations from field tests 26

2.3 Posiva 42

2.4 NWS 47

2.5 NWMO 50

3 Detailed research plan 51

3.1 Laboratory testing 51

3.2 Modelling 53

3.2.1 Charles University (SURAO) 53

3.2.2 SKB 53

3.2.3 NWMO 54

4 References 55

IGD-TP RELABEN Report D1 & D2

1 Introduction

The IGD-TP project “Stress relaxation of bentonite at high temperatures (RELABEN)“ has been established between the following national nuclear waste authorities: SURAO (Správa úložišť radioaktivních odpadů, Czech Republic), SKB (Svensk Kärnbränslehantering, Sweden), Posiva (Posiva Oy Olkiluoto, Finland), NWS (Nuclear Waste Services, UK) and NWMO (Nuclear Waste Management Organization, Canada). Its aim is to further investigate an important finding of the HITEC (Influence of temperature on clay-based material behaviour) work package of EURAD COFUND-EJP research project, which indicates strong thermal sensitivity of bentonite stress relaxation.

This report represents two planned deliverables of the RELABEN project, namely Deliverable 1 (SOTA based on HITEC updated SOTA, further review of the literature and experiments performed since the end of HITEC) and Deliverable 2 (Detailed research plan based on the knowledge gaps identified in Deliverable 1).

2 Initial state-of-the-art on bentonite rheological behaviour

2.1 Charles University (SURAO)

The rheological behaviour studied at Charles University to date has been presented in Najser and Mašín (2024) and Villar et al. (2025), to which the readers are referred to more details. The research results are summarised in following text.

2.1.1 BCV bentonite

Czech BCV bentonite extracted from the Černý Vrch deposit in the NW of the Czech Republic was used in this study. The bentonite is composed of Ca/Mg montmorillonite (70%), quartz (11%), kaolinite (5%), illite (4%), Mg-calcite (4%), goethite (3%) and anatase (2%). The interlayer cations in the montmorillonite consist mainly of Mg^{2+} and Ca^{2+} with some minor amounts of Na^{+} and K^{+} giving a total cation exchange capacity of 61 meq/100g.

The liquid limit of the bentonite reaches 135±5%, the plastic limit is 48±5% and the specific gravity is 2.76 g/cm^3. The bentonite is produced by Keramost a.s. in the form of powder with a typical size of aggregates of the order of tens of micrometers and the original gravimetric water content of 11%.

2.1.2 Experimental equipment

The experimental programme was performed in a special constant volume cell, denoted as T-MPC (from thermal multi-purpose cell) developed in-house at Charles University for high temperature testing (**Figure 1**). The high temperature cell consists of an externally heated confining ring with an internal diameter of 50 mm, top and bottom pistons. To minimise thermal expansion associated with high temperature changes, these high-temperature exposed components were made of invar. Constant volume conditions were ensured by an external high-rigidity steel frame, that held the pistons in a fixed position. Two PEEK (polyetheretherketone) thermal buffers were placed between the pistons and the frame to reduce heat transfer to the steel components. A small loadcell (manufactured by Burster GmbH) was positioned between the upper piston and the thermal buffer. Pressure and volume controllers with resolutions of 1 kPa and 1 mm^3 (type STDDPC, manufactured by GDS Ltd) were used throughout the experimental programme to control injection pressure, back pressure and conditions during the hydraulic conductivity measurement.

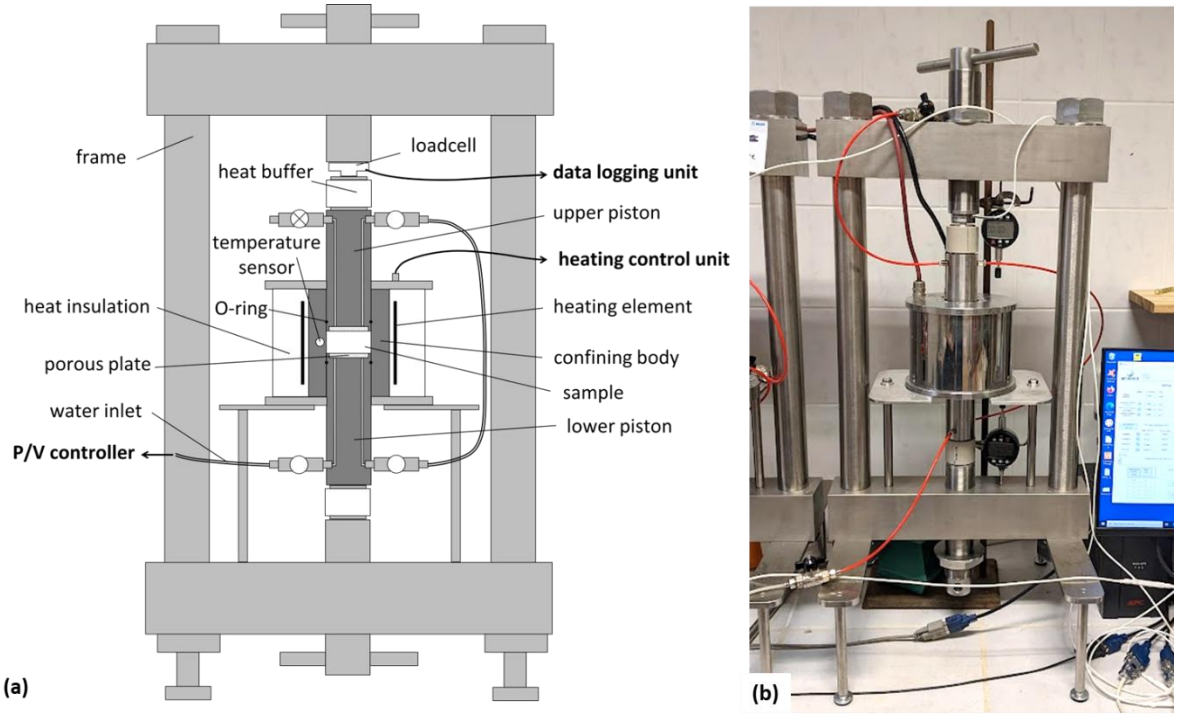

Figure 1: Configuration of the T-MPC cell. (a) - technical drawing (invar components are shown in dark grey; steel components are shown in light grey); (b) - actual photo.

Samples were prepared from bentonite powder with an initial hygroscopic water content of 11% by static uniaxial compaction in the central part of test cells. Firstly, the dependence of the dry density of the sample on the applied force was determined. The required compaction force was then controlled during compaction to maintain the best possible control over the initial dry density of the samples. Each sample was compacted from 36 g of bentonite.

The apparatus was exposed to high pressures and high temperatures during the tests, which typically induce deformation of the individual components due to thermal expansion and compressibility. They are rather small thanks to usage of invar components, but still not zero. Therefore, a careful calibration focusing on the PEEK thermal buffer and invar pistons was carried out prior to the start of the experimental campaign to assess any possible deviation from constant volume conditions. **Figure 2** shows the axial pressure development during the heating and cooling cycles applied to the test setup without the bentonite sample. In this arrangement, the two pistons acted against each other with the PEEK thermal buffer in place, and the system was mechanically preloaded to an axial pressure of 3.7 MPa, which is similar to the expected swelling pressure of the bentonite sample compacted to 1.6 g/cm^3. A temperature cycle of 20-100-20-50-20-150°C was applied in stages, with each stage held for several days.

The results show a considerable increase in axial pressure after heating. This is caused by the expansion of the invar pistons suppressed by the highly-rigid frame, which, despite the limited thermal expansion of invar compared to steel, significantly changes the axial pressure due to high invar stiffness. However, it is important to point out that this change in measured axial pressure in the setup without the sample immediately after heating practically does not affect the measured bentonite swelling pressures. This is because Young modulus of compacted bentonite is approximately 500-times smaller than that of invar, therefore, the pistons freely expand during heating when the bentonite sample is present, and no stresses are generated by this expansion when compared with the setup without bentonite, as bentonite volume change due to the piston expansion is negligible. The remaining effect which impacts the measured pressures is a slight increase of dry density of bentonite due to piston expansion. To quantify this effect, the thermal expansion of the pair of the pistons was measured directly for different temperatures, with a

maximum expansion of 0.07 mm at 150°C. This expansion results in only a 0.6% change in dry density, which has a minimal effect on the swelling pressures (this represents pressure change of 30 kPa following the pressure-dry density curve presented later in **Figure 3**). The key information, clear from **Figure 2**, is that the axial pressure measured once the cell has been heated remains constant and the difference in pressures measured before and after the heating-cooling cycle is negligible over the whole range of temperature cycles applied. The thermal expansion of the pistons and the resulting pressure change presented in **Figure 2** were not used to modify the swelling pressures obtained in the experimental programme, as the apparatus response is more complex (pistons are not heated homogeneously, invar cell changes its diameter), it is difficult to quantify and its effect is practically negligible, see reasoning above.

The calibration process also included the compliance of the PEEK thermal buffer at high pressures and temperatures, as well as proper quantification of the compliance of the loadcell and external frame. The deformation of the loadcell, thermal buffer and external frame after reaching the swelling pressure of each sample, although small, was used to more accurately determine the heights and dry densities of the samples presented in this paper (**Table 1**).

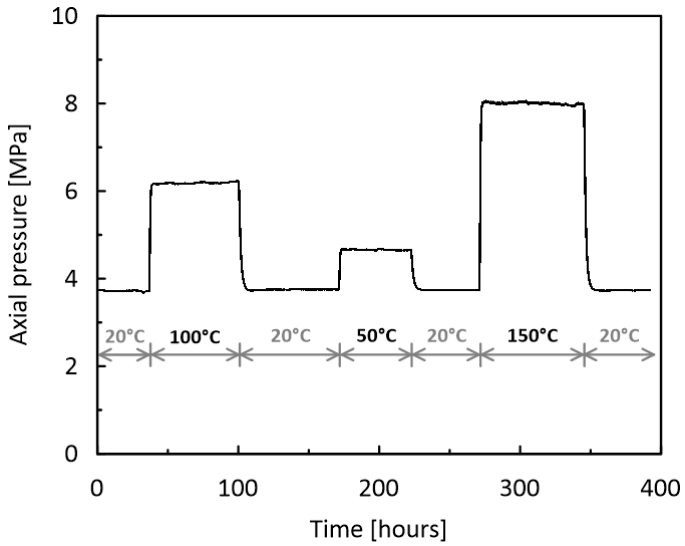

Figure 2: Effect of temperature change on measured axial pressure in T-MPC apparatus.

2.1.3 Testing programme

The aim of this study was to evaluate the effect of long-term high temperature exposure on the swelling pressure of bentonite samples. In order to analyze solely the effect of temperature, most samples were first fully saturated and then heated at constant volume under fully saturated conditions. Each test can be divided into three stages. In the saturation stage (stage I), the sample, fixed in its position by the external frame, was saturated from bottom side with distilled water using a small pressure gradient of 10 kPa at the laboratory temperature of 20°C. The increase in swelling pressure was monitored until full stabilisation, which was assumed to correspond to full saturation of the sample. The elevated temperature stage (stage II) started by a rapid heating of the sample cell to the target value (the position of the tubes and valves in stage II is presented in **Figure 1**). The temperatures applied to individual samples (50, 75, 100, 125 and 150°C) were kept constant for at least 28 days. In the final stage (stage III), the heating was switched off, the temperature in the cell was quickly reduced to 20°C and the test continued until the swelling pressure reached a constant value.

The tests carried out at lower temperatures (50 and 75°C) differed from the other tests in several aspects. Firstly, thermal buffers (see **Figure 1**) were not used in these experiments due to the relatively low temperature at the invar-steel interface. Secondly, no back pressure was applied in these tests as the applied temperature did not approach the boiling point of water. In the tests heated to 100, 125 and 150°C, a constant back pressure of 500 kPa was applied through pressure controller connected to both the top and bottom bases prior to heating to prevent boiling. The resulting pressure increase was subtracted from the measured value to obtain the swelling pressure.

Table 1: List of experiments including physical properties of samples and test conditions.

Sample	Applied T [°C]	Target ρ_d [g/cm^3]	Real ρ_d [g/cm^3]	Sample height [mm]	Back pressure [kPa]	Injection pressure [kPa]
1.6_T50	50	1.6	1.60	10.30	0	10
1.6_T75	75	1.6	1.54	10.71	0	10
1.6_T100	100	1.6	1.56	10.57	500	510
1.6_T125	125	1.6	1.55	10.68	500	510
1.6_T150	150	1.6	1.55	10.68	500	510
1.4_T150	150	1.4	1.39	11.87	500	510
1.8_T150	150	1.8	1.72	9.61	500	510
1.6_T150R	150	1.6	1.59	10.37	500	510

The test programme included five samples compacted to the target dry density of 1.6 g/cm^3, which were exposed to different temperatures (**Table 1**). A further two samples were compacted to target dry densities of 1.4 and 1.8 g/cm^3 and heated to 150°C to evaluate the effect of different dry density on swelling pressure development. Sample 1.6_T150R was subjected to a different test procedure with the order of the saturation and heating phases reversed. The sample was first subjected to an air back pressure of 500 kPa and then heated to 150°C. After five days it was saturated with distilled water through the bottom base using a pressure gradient of 10 kPa (**Table 1**). After a further 31 days, the heating was switched off and the test continued until the swelling pressure reached a constant value at 20°C.

At the end of the 1.6_T50, 1.6_T100 and 1.6_T150 tests, the hydraulic conductivity was measured to evaluate a possible difference to thermally untreated BCV samples. For this measurement, pressure and volume controllers were connected to the upper and lower piston and a pressure gradient of 400 kPa was applied, with pressures 420 kPa and 20 kPa maintained at the bottom and top of the sample respectively. The volume of water passing through the sample was recorded for 10 days and the hydraulic conductivity was calculated when constant flow through the sample was reached.

2.1.4 Results

The stage I of all tests except 1.6_T150R involved saturation of the samples under constant volume conditions. The final swelling pressures of the individual samples are presented in **Figure 3**. It shows that despite the careful preparation procedure, the samples prepared at the target dry

density of 1.6 g/cm^3 differed slightly in both actual dry density and swelling pressure. However, the swelling pressures are in reasonable agreement with earlier experiments on BCV bentonite. The comparison demonstrates that despite slightly lower swelling pressures, the results obtained from more complex T-MPC cells before heating are in reasonable agreement with the earlier results.

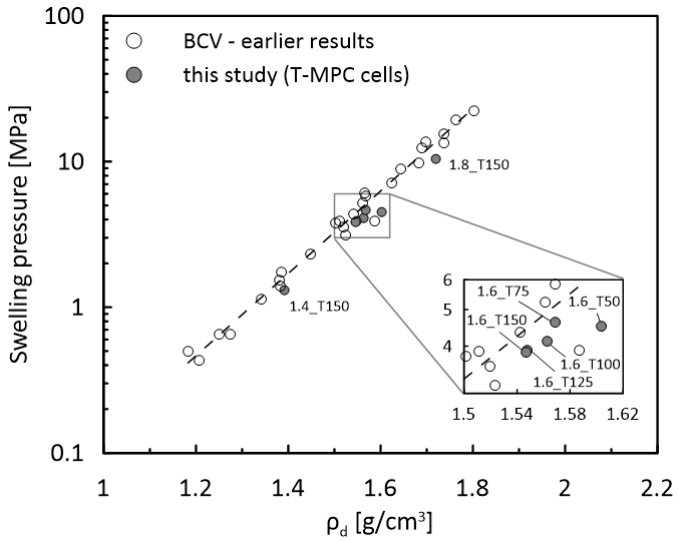

Figure 3: Comparison of swelling pressures after saturation with earlier experiments performed on BCV bentonite at room temperature up to date.

Temperature effect on the rate of stress relaxation

Five samples 1.6_T50 - 1.6_T150 with similar dry densities were studied to evaluate the effect of temperature on swelling pressure. The evolution of the swelling pressures during the tests exhibits similar trends (**Figure 4**). A sharp increase in axial pressure was observed immediately after heating at the beginning of stage II. This was followed by a decrease, which was also rapid in its initial phase, but which gradually slowed down. However, a decrease in axial pressure was measured for most samples throughout stage II. At the beginning of stage III, axial pressure decreased sharply. This was followed by a slower final recovery to a steady state value.

A comparison of the samples 1.6_T50 – 1.6_T150 shows that the decrease in swelling pressure during stage II was more significant at higher temperatures. In test 1.6_T50, the swelling pressure stabilised in approximately four days after heating. In tests heated to 75 and 100°C, the swelling pressure values also reached a steady state, but the time required for pressure stabilisation increased with increasing temperature. This was confirmed in test 1.6_T100, where stage II was extended to 48 days. On the other hand, above 100°C, especially in test 1.6_T150, the swelling pressure decreased continuously until the end of the stage II.

Cooling the samples in the initial part of stage III resulted in a sharp decrease associated with thermal shrinkage of the sample. The final swelling pressures measured at the end of stage III ($SP_{20°C\_fin}$) were significantly lower than the swelling pressures measured before heating at the end of stage I ($SP_{20°C\_ini}$). The magnitude of this decrease also clearly depends on the temperature applied in the stage II.

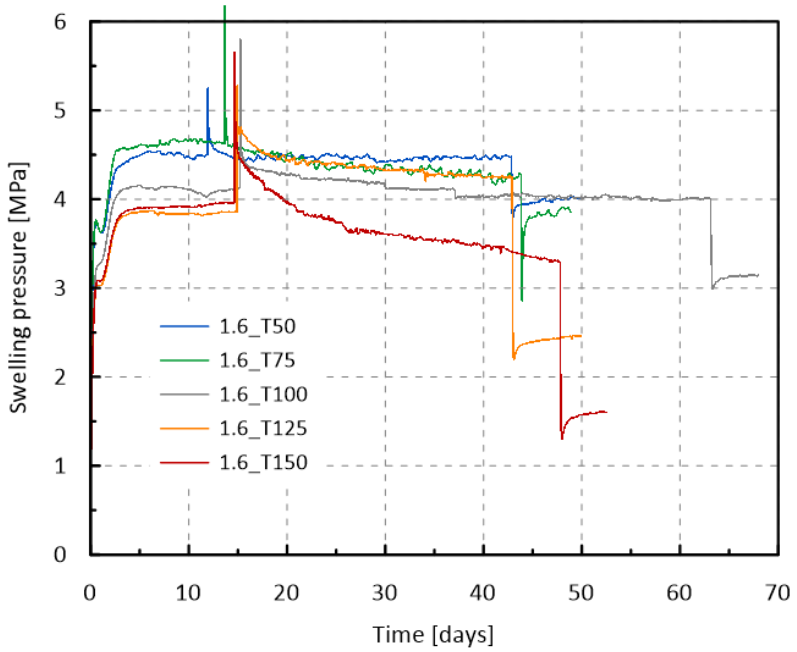

Figure 4: Development of axial pressure with time in samples compacted to 1.6 g/cm3, heated to 50°C– 150°C and subsequently cooled-down to 20°C.

A detailed view of the stage II in semilogarithmic plot is shown in **Figure 5**(a)**.** Test 1.6_T150 is presented as an example. The initial increase in swelling pressure is associated with the thermal expansion of the sample (bentonite grains and pore water). The excess pore water pressure generated by the heating dissipated through the porous stones on both sides of the samples.

In the following, the times required for the dissipation of the excess pore water pressure generated by the heating are estimated. This process is equivalent to pore water dissipation during consolidation. The time for full consolidation of the compacted BCV sample of the same dry density and height using the standard Casagrande method in an oedometric compression test was thus quantified, which yielded consolidation time of t = 10.5 hours. Taking into account the actual dynamic viscosity of water at a given temperature, the approximate time for complete dissipation of the excess pore pressure can be calculated using Eq. (1)

$$t_{100\_T} = \frac{t_{100\_20C}}{\left[\frac{\left(\frac{\gamma_{w\_T}}{\mu_T}\right)}{\left(\frac{\gamma_{w\_20C}}{\mu_{20C}}\right)}\right]} \qquad (1)$$

where t_{100_T} and t_{100_20C} represent the times for full dissipation of the excess pore water pressure at elevated and laboratory temperatures, respectively, γ_{w_T} and γ_{w_20C} represent unit weights of water at elevated and laboratory temperatures, respectively and μ_T and μ_{20C} represent dynamic viscosity of water at elevated and laboratory temperatures, respectively. The values of individual constants, along with the calculated dissipation times, are summarised in **Table 2**. It shows significant decrease of consolidation times with increasing temperature, which is caused by a decrease in dynamic viscosity of water. Direct measurement of pore water volume changes by pressure controllers during selected tests lead to excess pore water pressure dissipation times which are well with this calculation. In **Figure 5**(a), the time of the excess pore pressure dissipation estimated using oedometric consolidation is represented by the cross for one representative experiment. This time agrees well with the observed axial pressure evolution, indicating that the initial rapid increase and decrease of axial pressure in stage II of the experiments may be associated with heating-induced pore water pressure generation and its subsequent dissipation.

Table 2: Physical properties for calculation of time required for full dissipation of excess pore water pressure (t100_T) of the individual samples in the initial part of the stage II.

Temperature / Sample	t_{100_20C} [hours]	Dynamic viscosity μ [N·s·m^{-2}]	Water density ρ_w [kg·m^{-3}]	t_{100_T} [hours]
20°C	10.5	1.0016	998.2	10.50
1.6_T50	10.5	0.5465	988.1	5.79
1.6_T75	10.5	0.3774	974.8	4.05
1.6_T100	10.5	0.2816	958.4	3.07
1.6_T125	10.5	0.2276	938.9	2.54
1.6_T150	10.5	0.1864	916.7	2.13
1.4_T150	11.5	0.1864	916.7	2.33
1.8_T150	10.0	0.1864	916.7	2.03

From the moment of the excess pore water pressure dissipation, the samples were kept under constant conditions (volume, temperature, pore water pressure) until the end of the stage II. As no deformation of the apparatus was detected at elevated temperature (**Figure 1**), the continuous decrease in swelling pressure can only be attributed to the rheological behaviour of the sample. **Figure 5**b) compares the swelling pressure decrease in all tests compacted to the target dry density of 1.6 g/cm^3. In order to allow a better comparison, the swelling pressure decrease is represented by the ratio SP_{T_p0}/SP, where SP_{T_p0} represents the swelling pressure at full excess pore pressure dissipation (**Figure 5**a)). It shows a similar initial rate of relaxation for tests 1.6_T50 – 1.6_T125. However, in test 1.6_T50 the swelling pressure stabilised after four days and remained constant for the rest of the stage II. A significantly steeper slope was observed in test 1.6_T150.

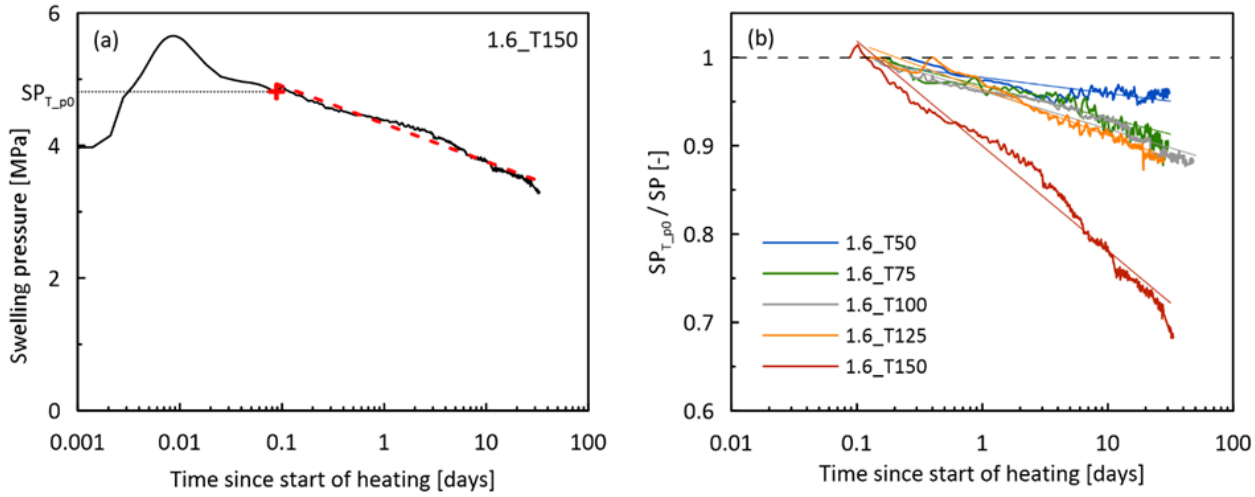

Figure 5: (a) - Example of swelling pressure evolution during stage II; (b) – comparison of normalised swelling pressure evolution in tests 1.6_T50 - 1.6_T150 in stage II after excess pore water pressure dissipation. Thin lines represent slopes used for Crel cal

The trends presented indicate that the decrease in swelling pressure can be approximately expressed by semilogarithmic regression, as indicated in **Figure 5**a)**.** The slope of the regression line, described as the coefficient of relaxation C_{rel}, was determined for the samples compacted to 1.6 g/cm^3 in a similar way to the definition of soil creep using Eq. (2)

$$C_{rel} = -\frac{\Delta SP}{\Delta log\ t} \qquad (2)$$

where ΔSP is the swelling pressure difference between the time of excess pore pressure dissipation (SP_{T_p0}) and the end of the stage II.

The trend of the C_{rel} change with the applied temperature for the individual tests is shown in **Figure 6**. It increases in the measured temperature range with a significant acceleration between 125 and 150°C. It should be noted that the C_{rel} values were determined from the whole interval between the excess pore pressure dissipation and the end of stage II as indicated by the trend lines in **Figure 5**(b). Sample 1.6_T50 exhibited a decrease in swelling pressure only during the first four days of stage II. The value of C_{rel} determined from this initial part, where thermal relaxation took place, is 0.19, which is a similar value to samples 1.6_T75 and 1.6_T100. On the other hand, the C_{rel} value of the 1.6_T150 sample increased in the last part of stage II. This means that the average values partly depend on the time of thermal exposure, especially in the case of the 1.6_T50 and 1.6_T150 samples.

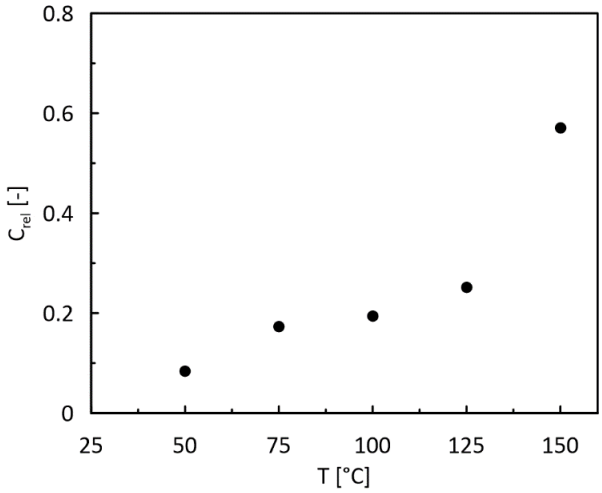

Figure 6: Variation of coefficient of relaxation with applied temperature in tests 1.6_T50 - 1.6_T150.

The decrease in the final swelling pressure determined at the end of the equilibration stage compared to the swelling pressure measured after saturation is analysed in **Figure 7**. It demonstrates a significant reduction of swelling pressure during stage II, which also increased with the applied temperature. It confirms that the relaxation process at elevated temperature induces permanent changes in the swelling pressure. It cannot be explained by the compliance of the apparatus due to the thermal cycle, as discussed in section 2. Sample 1.6_T50 maintained 90% of its initial value, whereas the swelling pressure of sample 1.6_T150 decreased to 41% due to high temperature exposure. The presented ratio may be slightly influenced by the incomplete relaxation within stage II in the samples exposed to temperatures above 100°C. It can be assumed that for these samples a longer thermal exposure could lead to an even more significant reduction in swelling pressure.

The saturation ratios of the samples at the end of stage III were determined by direct measurement of the water content, assuming a water density of 1.0 g/cm^3. The values ranged from 1.06 to 1.35 (**Table 3**). The calculated values of S_r higher than 1 can be explained by the fact that the actual water density in compacted bentonite is typically higher than 1.0 g/cm^3 (Jacinto et al., 2012). Desaturation of the samples at elevated temperature could be considered as a potential source of error of the presented measurements. It was assumed that constant gradient permeability tests would increase saturations, if the samples were desaturated during heating. However, no difference was observed between the saturation ratios of the samples subjected to hydraulic conductivity tests and the other samples. This indicates that the reduction in swelling pressure was not due to desaturation of the samples during stage II.

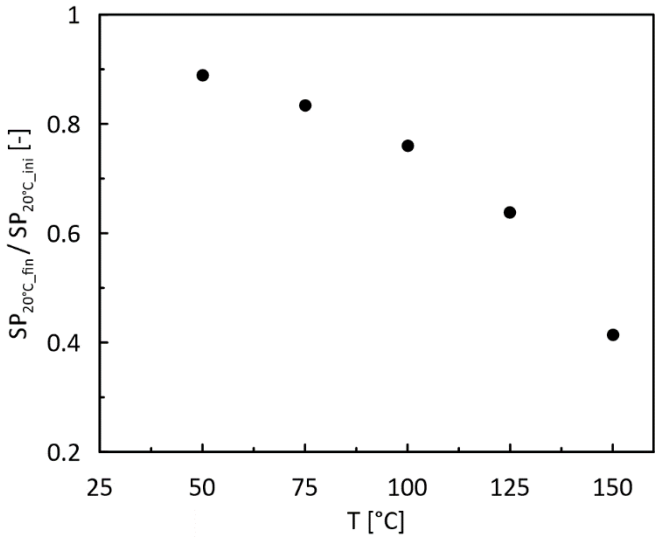

Figure 7: Decrease in swelling pressure due to thermal treatment, expressed as the ratio of the final swelling pressures at the end of the test (SP20°C_fin) to the initial swelling pressure determined after saturation (SP20°C_ini).

Effect of dry density on thermal relaxation

The effect of dry density was investigated on samples 1.4_T150, 1.6_T150 and 1.8_T150 compacted to different dry densities (**Table 1**), which generate significantly different swelling pressures (Table 3). A significant thermal relaxation was observed with a considerable decrease in the final swelling pressures at the end of the tests compared to the swelling pressures after saturation. The final swelling pressure reached 58% of the initial value for the 1.8_T150 test and 42% for the 1.4_T150 test, which is similar to 41% of the initial swelling pressure reached in the 1.6_T150 test.

Table 3: Summary of the main results. SP20°C_ini refers to the swelling pressures measured at the end of stage I, SPT_fin are swelling pressures at the end of stage II and SP20°C_fin are swelling pressures measured at the end of stage III.

Sample	Swelling pressure [MPa]			$SP_{20°C\_fin}$ / $SP_{20°C\_ini}$ [-]	Hydraulic conductivity k [m/s]	S_r [-]
	$SP_{20°C\_ini}$	SP_{T_fin}	$SP_{20°C\_fin}$			
1.6_T50	4.51	4.48	4.01	0.89	$1.3 \cdot 10^{-13}$	1.16
1.6_T75	4.62	4.26	3.86	0.83	-	1.15
1.6_T100	4.13	4.00	3.14	0.76	$2.7 \cdot 10^{-13}$	1.25
1.6_T125	3.85	4.25	2.46	0.64	-	1.19
1.6_T150	3.91	3.29	1.62	0.41	$1.9 \cdot 10^{-13}$	1.18
1.4_T150	1.31	0.97	0.55	0.42	-	1.06

1.8_T150	10.41	8.71	6.08	0.58	-	1.35
1.6_T150R	-	2.40	1.68	-	-	1.23

The rate of relaxation of all three experiments is plotted in **Figure 8**. Despite different values of swelling pressure, all samples exhibit a similar rate of relaxation with slightly faster progress in the initial part for the low dry density sample. In the semilogarithmic plot, all curves deviate from the linear trend such that the tangent C_{rel} slope increases with time.

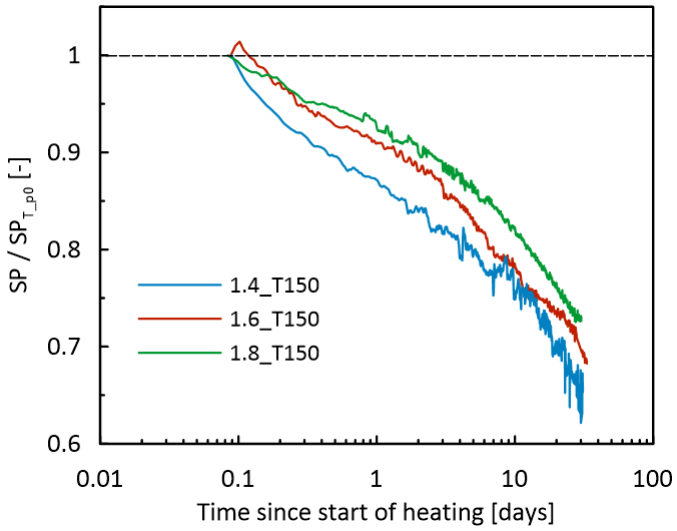

Figure 8: A comparison of the normalised swelling pressure development in tests 1.4-1.8_T150 in the stage II after excess pore water pressure dissipation.

Further to the specific tests described above, a cyclic heating-cooling experiment (denoted as T72) has been performed at Charles University. After saturation, the sample of the initial dry density of ρ_d = 1.55 g/cm^3 was heated in steps from 20°C through 50°C and 100°C to 150°C. Subsequent cooling-heating cycles 20°C-150°C-20°C-150°C-20°C were applied, see Villar et al. (2025) for more details. The swelling pressure evolution is shown in **Figure 9**, demonstrating both stress relaxation and significant stress decrease in the cooling periods. The experiment is valuable for constitutive model development and validation, see Mašín (2025) for its finite element simulations with advanced constitutive model VIBE (see Sec. 3.2.1 for more details).

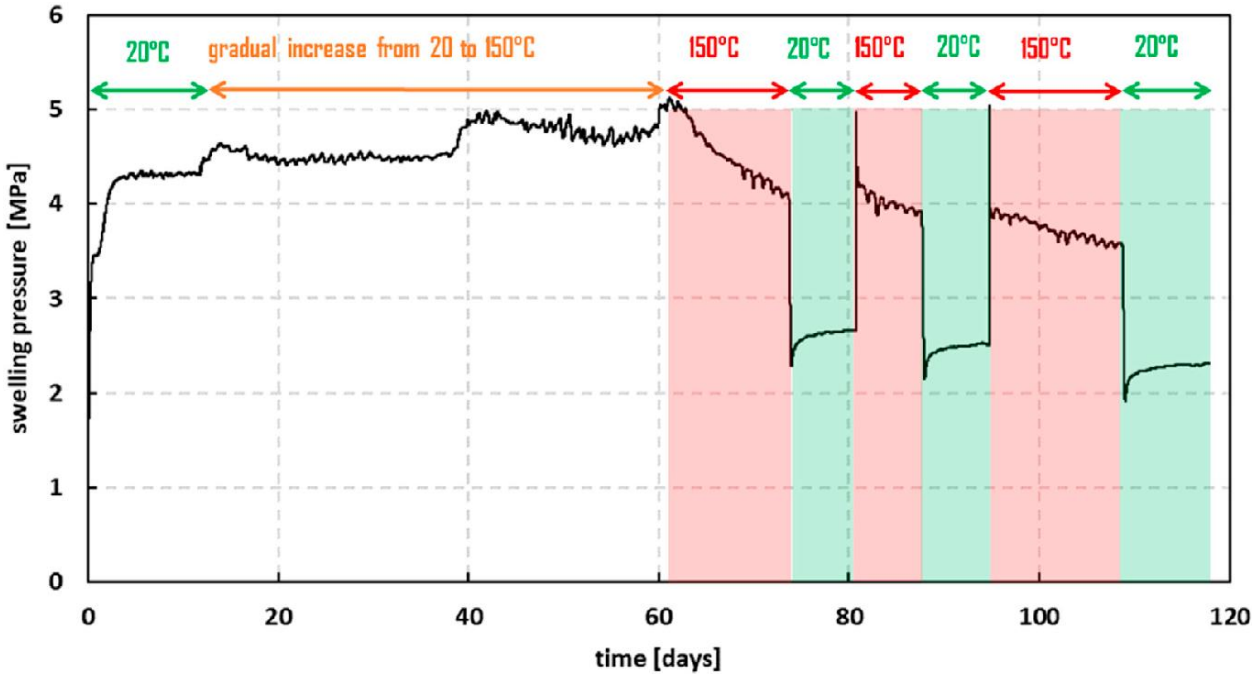

Figure 9: Cyclic heating-cooling experiment T72 on BCV bentonite performed at Charles University, see Villar et al. (2025) for details.

Effect of order of saturation and heating phases

Two samples with the same target dry density and temperature applied in the heating stages were tested with different order of saturation and heating phases (sample 1.6_T150R was heated at as-compacted conditions and saturated subsequently, which better represents the conditions in the repository). The development of swelling pressures in both tests is compared in **Figure 10**. The axial pressure in test 1.6_T150R increased after heating due to soil and microstructural water thermal expansion. However, within a few days of heating, the axial pressure gradually disappeared. Thermal relaxation thus took place even in the unsaturated state, which is in agreement with Kuhn and Mitchell (1993) who indicated that wet and dry clays exhibit qualitatively similar creep behaviour. Saturation of the sample induced rapid increase in swelling pressure. Despite a slightly higher dry density compared to sample 1.6_T150 (Table 1), the swelling pressure reached a significantly lower value, which may be attributed to stress relaxation prior to saturation. The rate of swelling pressure reduction during the high-temperature stage showed a similar trend for both samples. The final swelling pressures after cooling were similar for both experiments. This comparison indicates that the order of the saturation and heating phases has no impact on the swelling pressure decrease at high temperature.

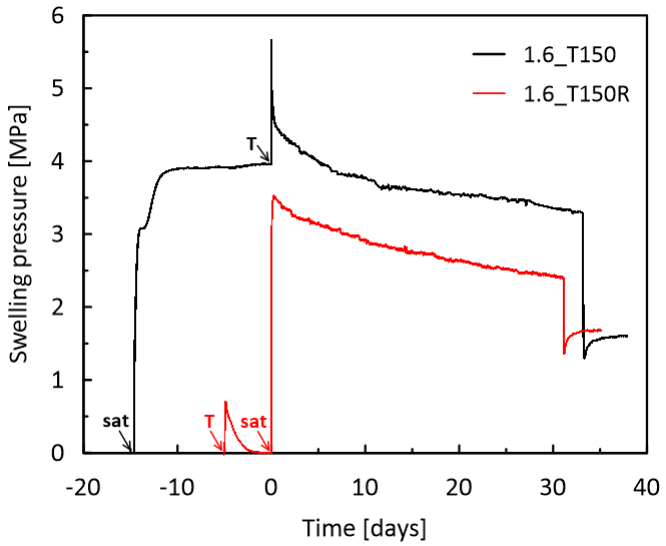

Figure 10: Comparison of tests with different order of saturation (sat) and heating (T) phases.

Hydraulic conductivity after heating-cooling cycle

The hydraulic conductivity of samples 1.6_T50, 1.6_T100 and 1.6_T150 was determined at room temperature at the end of these tests to evaluate the effect of the thermal treatment on the sealing function of the bentonite. **Figure 11** shows the measured hydraulic conductivities compared to the typical trend of hydraulic conductivity obtained for untreated BCV bentonite (Svoboda et al., 2022). The results show good agreement between the data sets, indicating that exposure to high temperatures and associated thermal relaxation did not cause a measurable change in hydraulic conductivity. No trend in hydraulic conductivity was observed with respect to the temperature applied during stage II.

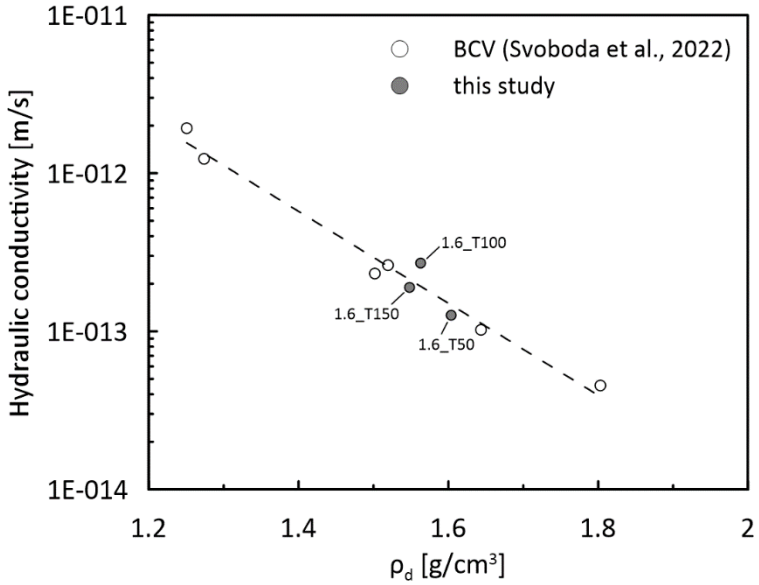

Figure 11: Hydraulic conductivity of the samples previously exposed to high temperatures and its comparison with thermally untreated BCV samples.

2.2 SKB

The effect of thermal relaxation of bentonite has not been specifically studied by SKB. There have however been studies in related areas which can be of value for the RELABEN project. These are:

- A study with a large set of laboratory tests was performed where fully water saturated samples of bentonites was exposed to temperatures in the range –10°C to +25°C. The swelling pressure response was recorded continuously. The samples were varied with respect to bentonite type (e.g. calcium or sodium dominated), smectite content and density. This study is reported in Birgersson et al (2010).
- Studies of swelling pressure of bentonite samples that have been retrieved from field tests where they have been exposed to elevated temperatures for long periods of time. This is reported in: Karnland et al 2009a, Svensson et al 2011, Olsson et al 2013, Svensson et al 2023 and Svensson et al 2024.

A summary of the relevant aspects of the studies is given in this section.

Freezing of bentonite

The overall objective of the study presented in Birgersson et al 2010 was to study the behavior of compacted bentonite below 0°C. It was investigated how swelling pressure (i.e. sealing properties) changes with temperature and under what conditions bentonite freezes.

A set of bentonite samples were prepared in cylindrical test cells of constant volume. The main choice of bentonite in this study is the sodium dominated MX-80 bentonite. Samples of MX-80 bentonite in a span of densities corresponding to swelling pressures between 1–30 MPa were chosen. To study a Ca/Mg-dominated system a sample of Deponite-Can bentonites was also tested. Furthermore, bentonites of lower quality are of interest to use as e.g. backfill material and therefore two such materials were tested: Kutch Backfill (Ku-BF), which is more sodium dominated, and Milos Backfill (Mi-BF) which is more calcium/magnesium dominated. The bentonites are summarized in Table 4. Samples of materials other than bentonite were also prepared in order to separate the general pressure response effects in systems containing water from the bentonite specific ones. The other materials chosen to investigate for this purpose was a silt powder (feldspar) which represents a conventional porous system and gravel with pores on the mm-scale. Bentonite powder (or silt powder or gravel) was compacted directly in the cells, schematically pictured in **Figure 12**. Different types of test cells were used which had a diameter of either 20 mm or 35 mm and consisted of steel, titanium, PEEK or combinations thereof. The cells were closed, the height adjusted to 10 mm and contacted with deionized water via sintered filters at room temperature. The cells were equipped with force transducers (sensotech model 53) which sampled the confining force axially (see **Figure 12**) with a frequency of 1/20 min–1 (occasionally a higher frequency was used). The silt and gravel samples were water saturated by applying a small water pressure on one side of the cells (i.e. they were flushed) while the bentonite samples were saturated spontaneously when contacted with water due to their swelling ability. In the case of bentonites, the saturation process was carefully monitored by measuring the swelling pressure build-up.

Table 4 Bentonites tested. Material data from Karnland et al 2006 and Olsson and Karnland 2009.

Name	Montmorillonite content (%)	%Na	%Ca	%Mg
MX-80	80-85	70-80	15-20	6-8
Deponit-CAN	~80	24	45	29
Milos backfill	58	8-10	40-41	47-49
Kutch backfill	78	55-56	31	13-14

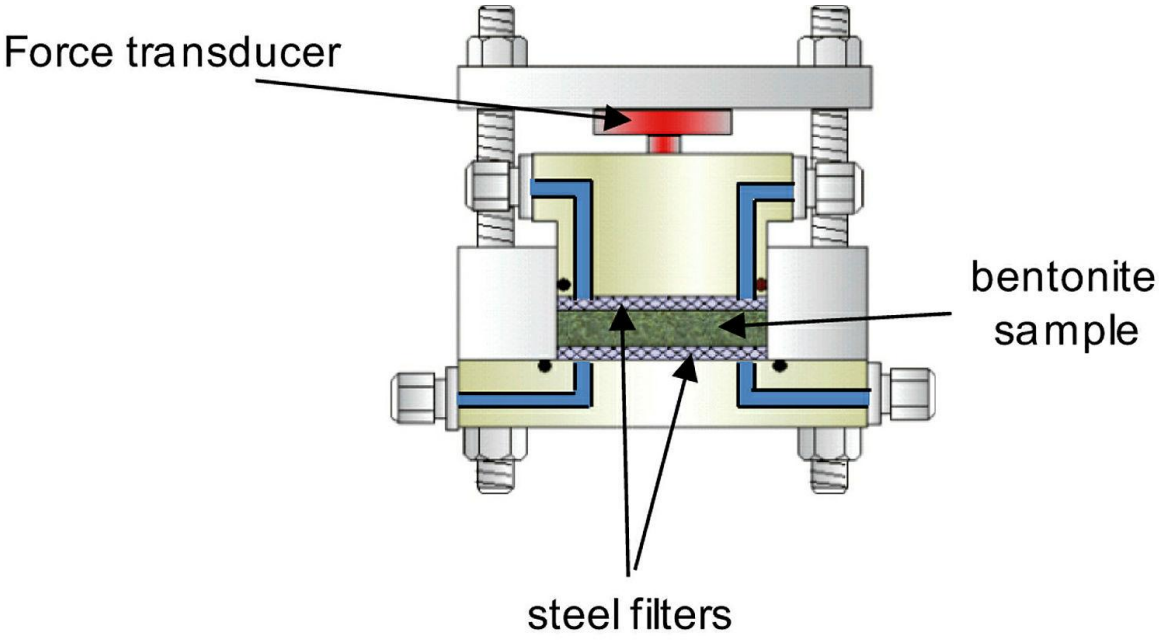

Figure 12: Schematic picture of the test cell (Birgersson et al 2010).

The fully water saturated samples were disconnected from their external water supply and placed in a cooled incubator (Sanyo MIR-153) in which temperature could be kept constant in the interval –10°C to +50°C. The samples, however, where still in contact with external water because the channels and filters of the test cells still contained water. The temperature was measured separately by a sensor in the incubator. The pressure sensors, however, produce some heat. The measured incubator temperature thus does not exactly correspond to sample temperature. Furthermore, by the same reason it cannot be excluded that a weak temperature gradient is imposed over the sample. The samples were exposed to different temperatures and their pressure response recorded. The testing was done in cycles of freezing and thawing. Some of these cycles had to be rather long (>100 days) in order to achieve pressure equilibrium. During this amount of time the incubator occasionally had to be defrosted to function properly. During the defrosting, the samples were stored in a cooled isolated box, in which temperature was not controlled. The bentonite test cells were flushed with water after a freezing/thawing cycle in order to maintain external water in the system.

The pressure response due to temperature changes of the test cells alone containing a steel dummy sample is pictured in **Figure 13**. This figure also exemplifies the general way pressure- vs. time graphs are presented. The measured incubator temperature is plotted together with the

relevant sample pressure. Temperature is always read on the right-hand y-axis. Sample material and sample ID (see **Table 5**) is written in the legend.

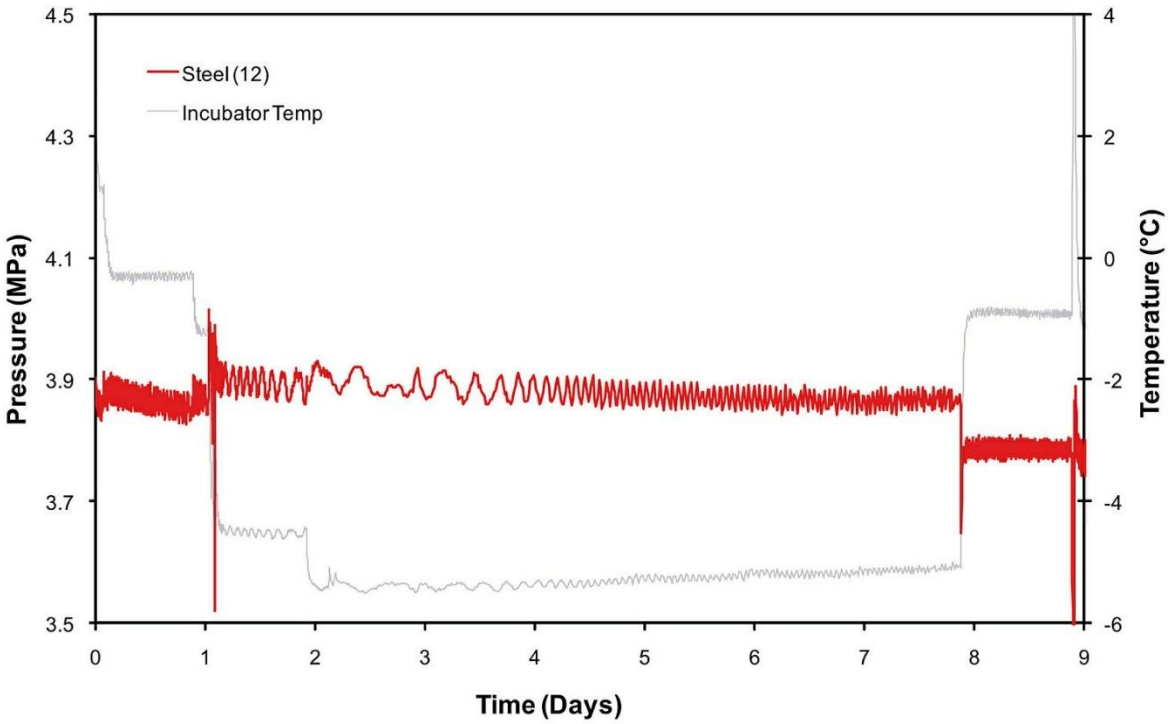

Figure 13: The pressure response due to temperature changes of a test cell containing a dummy steel sample (sample 12 in Table 2 1) during freezing cycle 1. The temperature peak seen around day 9 is due to a defrost of the incubator after the end of the freezing cycle (Birgersson et al 2010).

Table 5: Samples tested. The samples are foremost characterized by their swelling pressure at 0°C, P_s^0. Listed is also the diameter, D, of the samples. All samples were of height

10 mm. After termination also water/solid mass ratio, w, was determined (Birgersson et al 2010).

Sample ID	Material	P_s^0 (MPa)	D (mm)	Started	Ended	Cycles	*w*
Freezing01	MX-80	6–7	20	2007-06-19	2009-06-25	1,2,3,4,5,6,7	0.29
Freezing02	MX-80	5	35	2007-06-19	2007-06-28	1	n.d.
Freezing03	MX-80	5	20	2007-06-28	2008-04-08	2,3,4	0.33
Freezing04	MX-80	4	20	2007-06-28	2008-04-08	2,3,4	0.32
Freezing05	MX-80	1	20	2007-10-05	2008-06-05	4,5 (partly)	0.42
Freezing06	MX-80	30	20	2007-10-05	2009-03-13	4,5	0.21
Freezing07	Dep-Can	6	20	2008-04-23	2009-06-25	5,6,7	0.29
Freezing08	Mi-BF	2	20	2008-04-23	2009-05-27	6,7	0.33
Freezing09	Ku-BF	9	20	2009-04-23	2009-03-13	5	0.35
Freezing11	Feldspar silt	–	20	2007-06-19	2007-09-03	3	–
Freezing12	Steel	–	20	2007-06-19	2007-06-28	1,2,3	–
Freezing13	Feldspar silt	–	35	2007-06-19	2007-06-28	1	–
Freezing14	Steel	–	35	2007-06-19	2007-06-28	1	–
Freezing15	Gravel	–	20	2007-06-28	2007-09-03	1,2,3	–

Looking at the response above 0°C, seen e.g. in **Figure 13** shows that it is very accurate and fast (as compared to systems below 0°C). The three samples in **Figure 14** show an equilibration time in the order of an hour or less and have a small drop of equilibrium swelling pressure with increasing temperature. In **Figure 15** the equilibrium pressures are plotted as a function of temperature. This diagram is produced by making average values of temperature and pressure on the plateaus seen in **Figure 14**. In **Figure 15** is also plotted the direction in which temperature changes was made, i.e. if going towards higher or lower temperatures. It is seen that a consistent difference in slopes prevails dependent on the direction; when decreasing temperature, the slope is a little larger for all three samples. The reason for this path dependence will not be addressed here (it could be associated with the generally observed swelling pressure hysteresis but could also be an artifact caused by equipment). Regardless of this complication, it is evident from **Figure 15** that the slope of the Ps-T-line is larger for samples with higher pressure, i.e. with higher density. In **Figure 16** is shown the pressure response due to temperature above 0°C of a bentonite sample of the same type (MX-80) but with lower density. It is very interesting to see that at this density, the equilibrium pressure response for MX-80 bentonite is opposite to what was observed for the samples in **Figure 15** – here an increased temperature gives an increased equilibrium pressure. This specific sample was flushed with water in the presented time interval which is seen to give a small pressure response. However, the same type of pressure response due to temperature was observed also after rewetting. A corresponding Ps-T-diagram for this sample is shown in **Figure 17**. The pressure response above 0°C for a MX-80 bentonite sample in the opposite limit of high density is shown in **Figure 18** and **Figure 19**. Note the significantly more pronounced slope of the high density sample in **Figure 19** as compared to the samples in **Figure 15**. In **Figure 20** and **Figure 21** are shown equilibrium pressure versus temperature curves also for Deponite-Can and Mi-BF samples above 0°C.

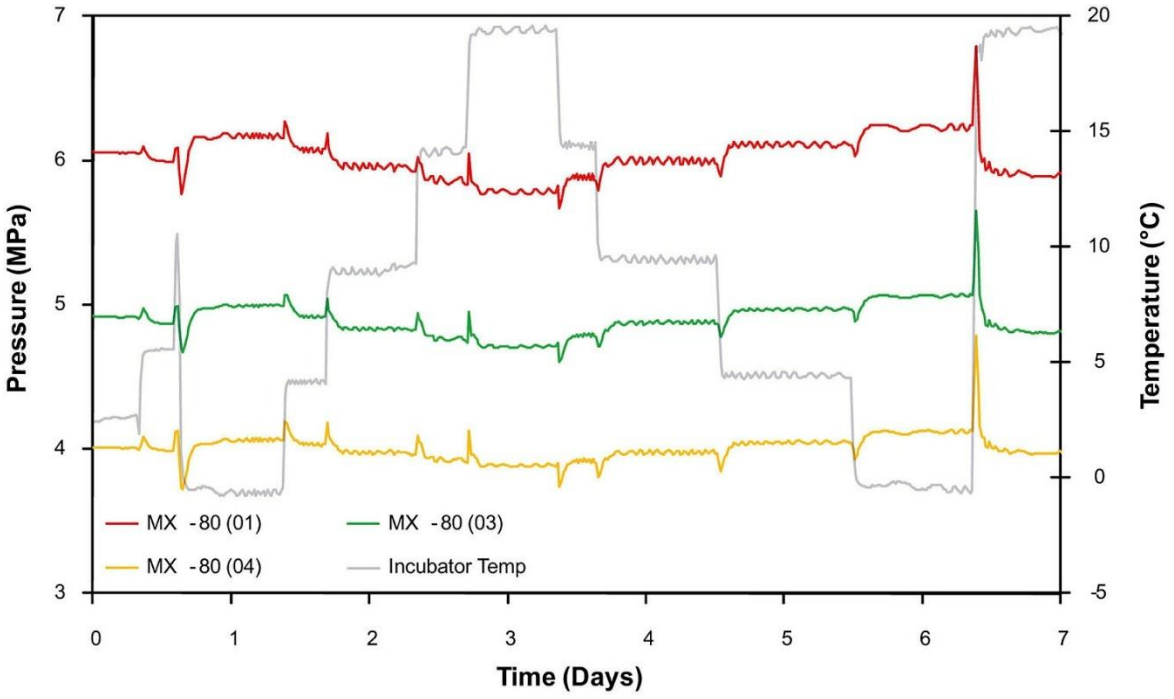

Figure 14: Pressure response of three bentonite samples above 0°C recorded after freezing cycle (Birgersson et al 2010).

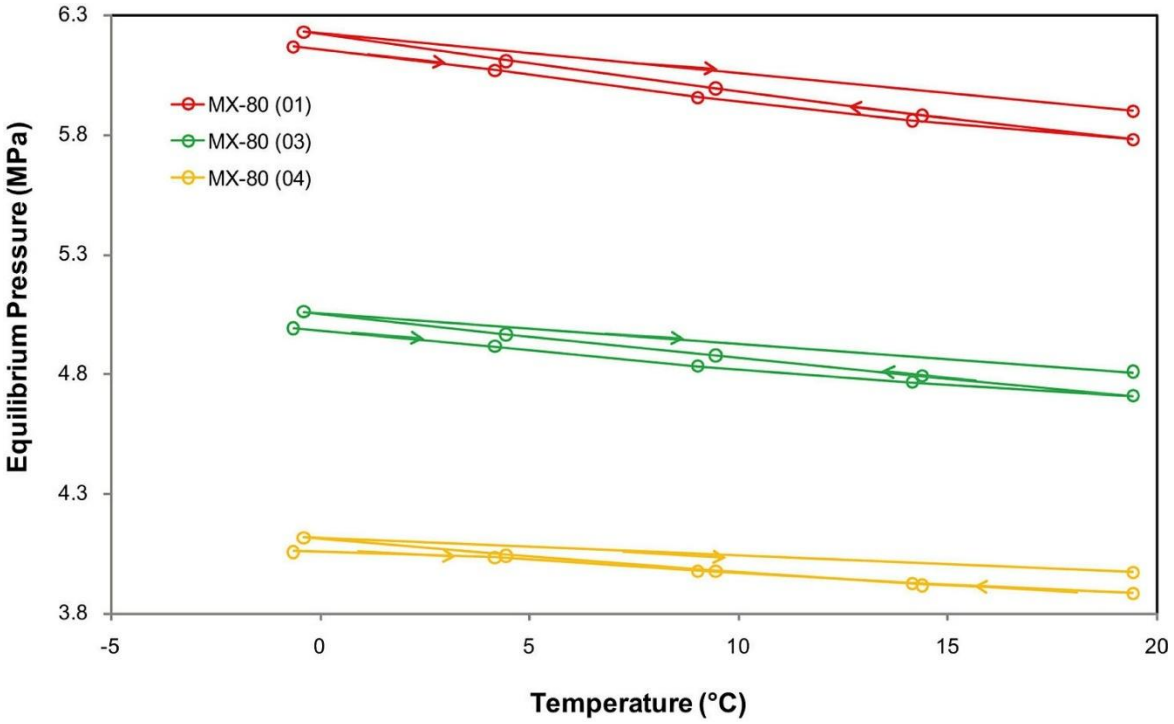

Figure 15: Equilibrium swelling pressure of three MX-80 bentonite samples as a function of temperature above 0°C. The plots are produced by making averages of the time series shown in **Figure 14**. Arrows indicate the direction of the temperature changes. The Ps-T curve is negative for all three samples and with an increasing slope for higher densities. Note that the slopes are systematically larger in all three

samples when going from higher to lower temperatures (i.e. when pressure increases) (Birgersson et al 2010).

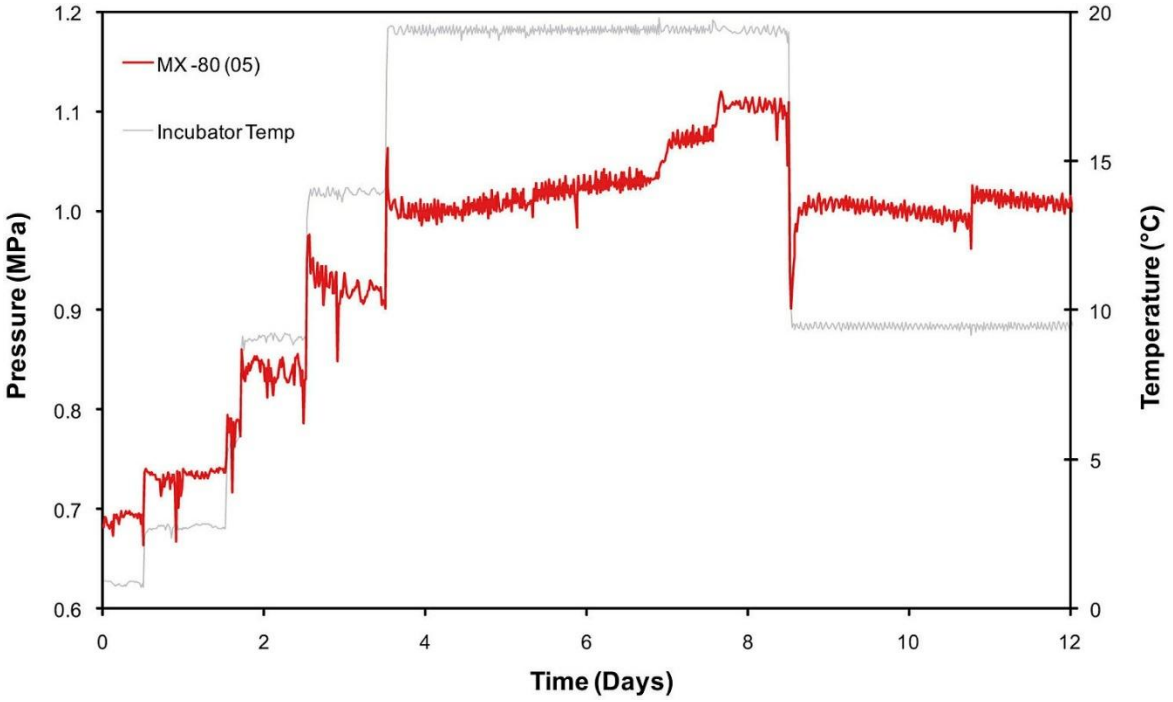

Figure 16: Pressure response of a low density MX-80 bentonite sample above 0°C recorded after freezing cycle 4. Note that this sample was flushed with water at day 7 and day 11, which gives small pressure responses. It is however clear that a positive temperature response is seen in this sample as the same type of response is seen both before and after flushing (Birgersson et al 2010).

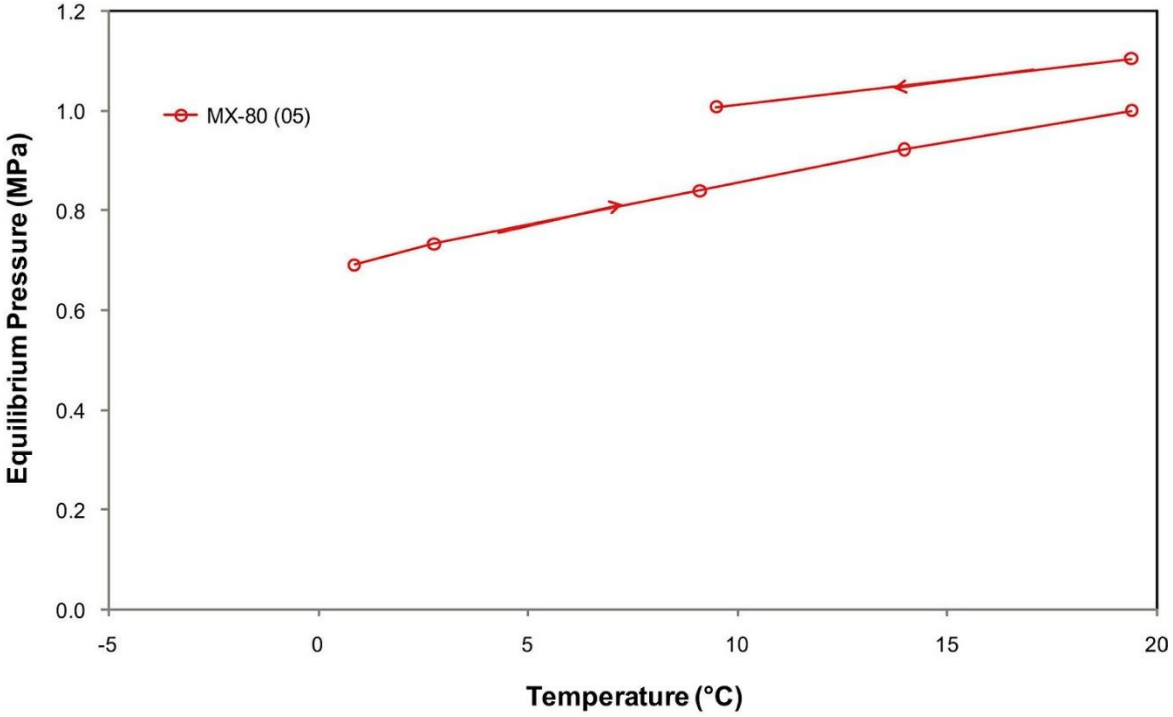

Figure 17: Equilibrium swelling pressure as a function of temperature above 0°C of a low density MX-80 bentonite samples. Note that the slope is positive in contrast to MX-80

samples of higher density (cf **Figure 16**). The Arrows indicate the direction of the temperature changes. The data is sampled after freezing cycle 4 (**Figure 16**) (Birgersson et al 2010).

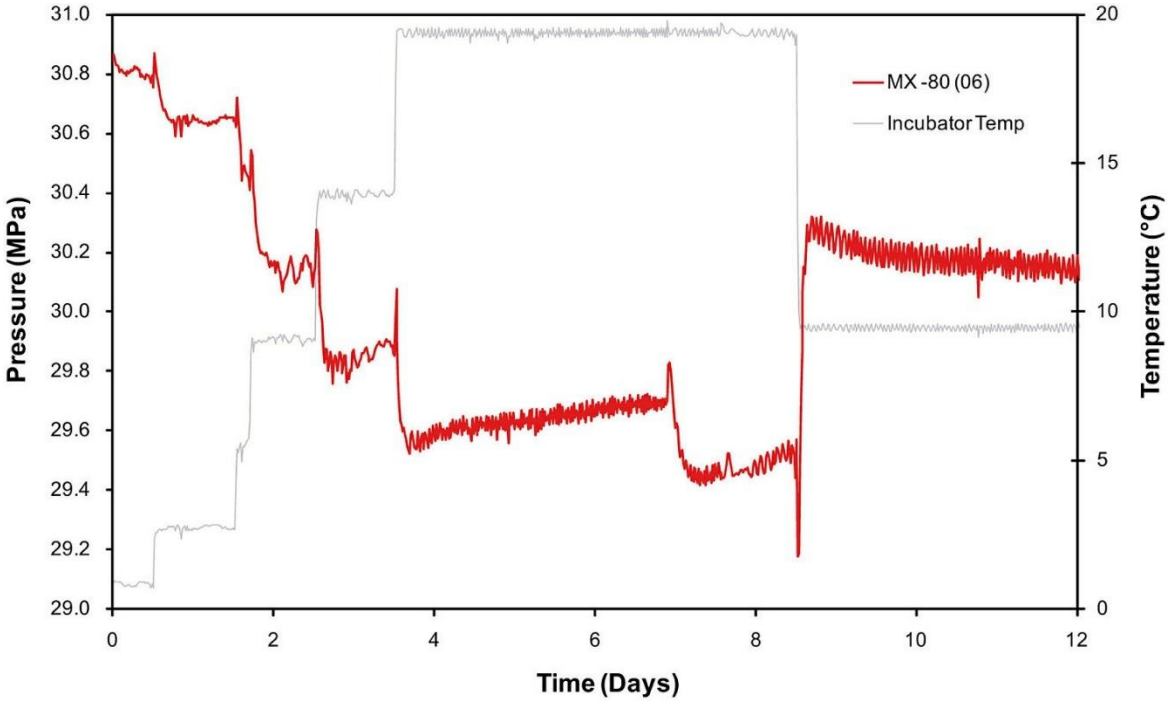

Figure 18: Pressure response of a high density MX-80 bentonite sample above 0°C recorded after freezing cycle 4. The sample was flushed with water at day 7 and day 11 (Birgersson et al 2010).

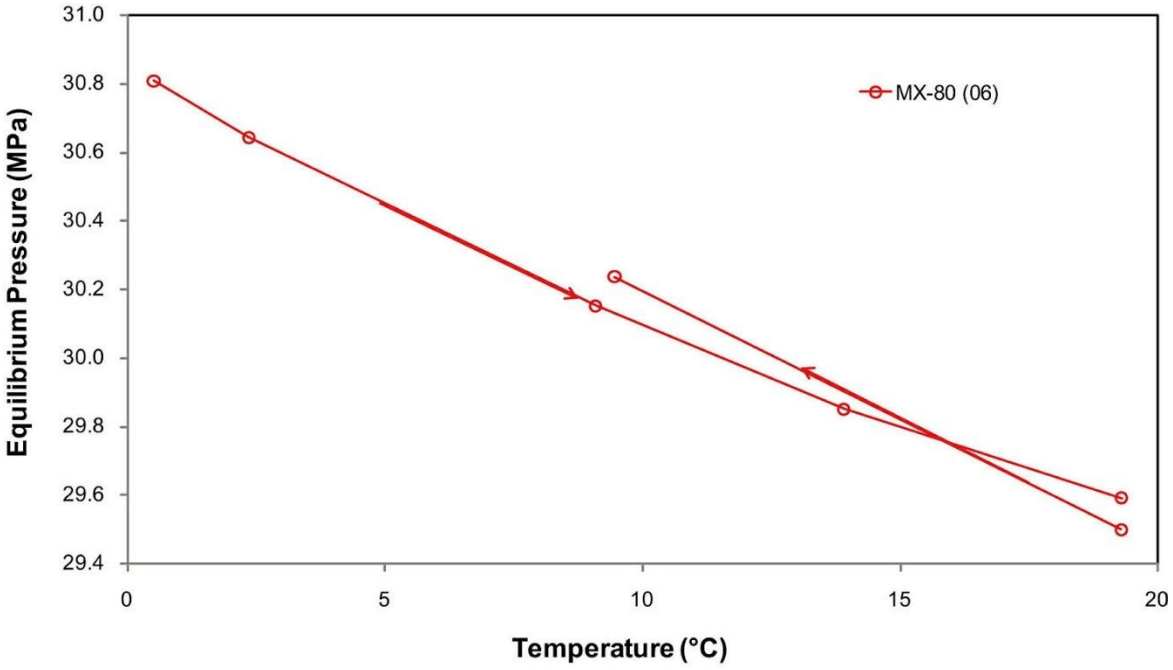

Figure 19: Equilibrium swelling pressure as a function of temperature above 0°C of a high density MX-80 bentonite sample. Arrows indicate the direction of the temperature

changes. The data is sampled after freezing cycle 4 (**Figure 18**) (Birgersson et al 2010).

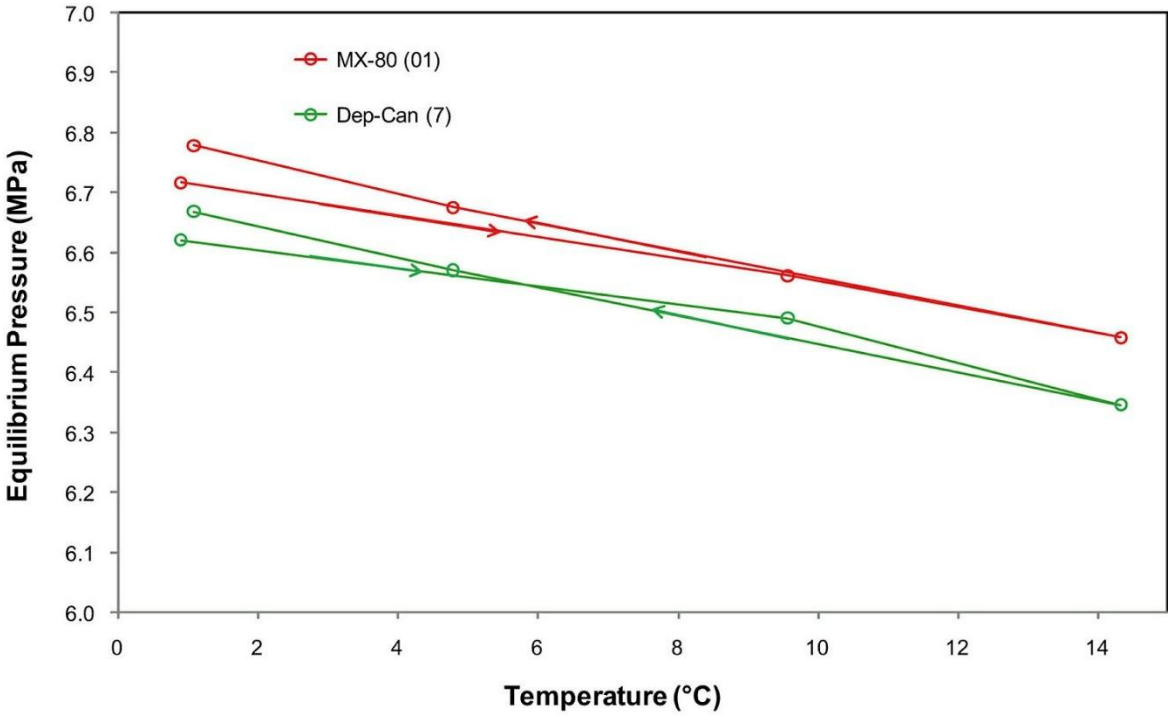

Figure 20: Equilibrium swelling pressure as a function of temperature above 0°C of an MX-80 bentonite sample and a Deponite-Can bentonite sample of comparable

densities.Arrows indicate the direction of the temperature changes. The data is sampled after freezing cycle 6 (Birgersson et al 2010).

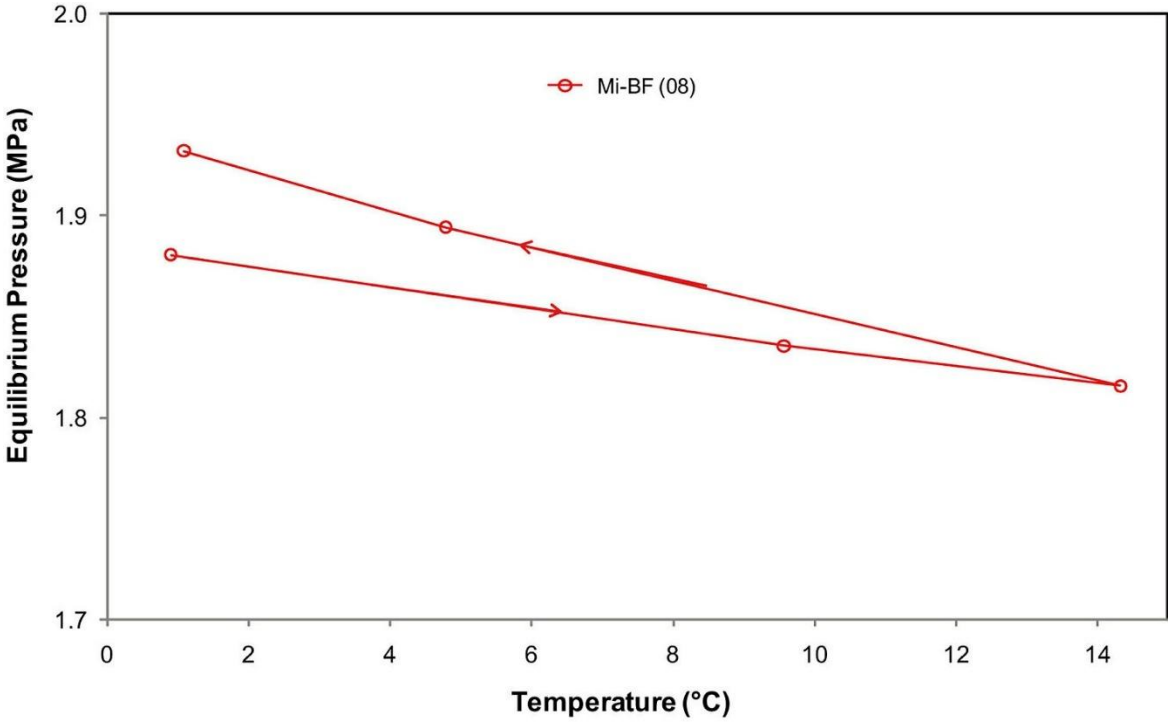

Figure 21: Equilibrium swelling pressure as a function of temperature above 0°C of an Mi-BF bentonite sample. The arrows indicate the direction of the temperature changes. The data is sampled after freezing cycle 6 (Birgersson et al 2010).

The tests at temperatures above 0°C show that the swelling pressure decreases with increasing temperature for all tests except MX-80 (5). MX-80 (5) had the lowest density and the target swelling pressure was 1 MPa. The Mi-BF (08) test had a target swelling pressure of 2 MPa and here there is a decrease, albeit small, in swelling pressure with temperature. A general observation is that the decrease in swelling pressure as a function of temperature increases with increasing dry density.

All tests above 0°C show an increase in swelling pressure as a result of thermal cycling. No thermal relaxation is observed in this temperature range.

Observations from field tests

LOT

The LOT test series at the Äspö Hard Rock Laboratory (HRL) were focused on identifying and quantifying such mineralogical alterations in the bentonite exposed to typical repository-like conditions. In total, the LOT project included seven test parcels, which contain a central Cu-tube surrounded by cylindrical bentonite blocks with a diameter of 30 cm, and gauges for temperature, total pressure, water pressure and humidity. Electrical heaters placed inside the copper tube were used to simulate the heat generation from the decaying spent fuel. Three parcels were exposed to standard KBS-3 conditions (maximum temperature below 100°C) and four parcels to adverse conditions (maximum temperature below ~140°C). Both the standard and the adverse test series includes short term tests (1 to 2 years), medium term tests (>5 years) and long term tests (>10 years). Karnland et al 2009a concerned the A2 test parcel, which was a medium term test exposed to adverse conditions. The hydraulic conductivity and swelling pressure were determined in

combined tests on material chosen from strategic positions within the test parcel and on the corresponding reference material. The test series includes the following sub-series:

- reference material, air-dried and compacted, Äspö-water, 6 samples,
- parcel material, air-dried, crushed and recompacted to buffer density, Äspö-water, 6 samples,
- parcel material, naturally saturated, sawn and trimmed to fit the test cells, Äspö-water, 6 samples.

Six purpose-built swelling pressure test cells were used (**Figure 12**). The samples were confined by cylinder rings with a diameter of 20 mm and stainless-steel filters at the top and bottom. The test volumes were sealed by o-rings placed between the bottom plates and the cylinder rings and between the pistons and the cylinder rings. At test start the height of the test volumes were fixed to 10 mm by the flanges on the moveable pistons. The axial force from the sample was determined by the transducer placed between the piston and the upper lid. The displacement of the piston due to transducer deformation is 100 µm at maximum force, which consequently correspond to 1% of the sample height and is considered insignificant.

Reference samples were prepared from material saved from block production. Parcel samples were prepared from extracted material in two ways,

- air-dried and crushed to a grain size like the original MX-80 powder and re-compacted to a density of 2,000 kg/m^3,
- sawn by a cylindrical saw and trimmed to fit the test cells and thus had a density close to but slightly lower than the field value.

Äspö ground water was initially circulated below the lower filter to let air out through the upper filter during the saturation. The water uptake was indirectly monitored by the force transducer (**Figure 12**). At constant swelling pressure, the solution was circulated also above the upper filter. Stable force conditions were reached within 1 week. At this point a water pressure of maximum 50% of the measured swelling pressure was applied in the bottom filter to establish percolation. The volumes of the percolated water solution were registered daily by visual observations of the water/air interface meniscus. The water pressure was thereafter reduced to zero and the tests were terminated when the recorded axial forces had stabilized.

The scatter in density of the sawn and trimmed samples are likely due to the preparation technique and are not directly related to the previous field conditions (**Figure 22**). No differences were found in the results from warm positions compared to those from the upper cool positions or from the reference material. The results from the A2 parcel are also in good agreement with previously measured results, e.g. from the short term test parcel A0 and reference material (Karnland et al. 2009b).

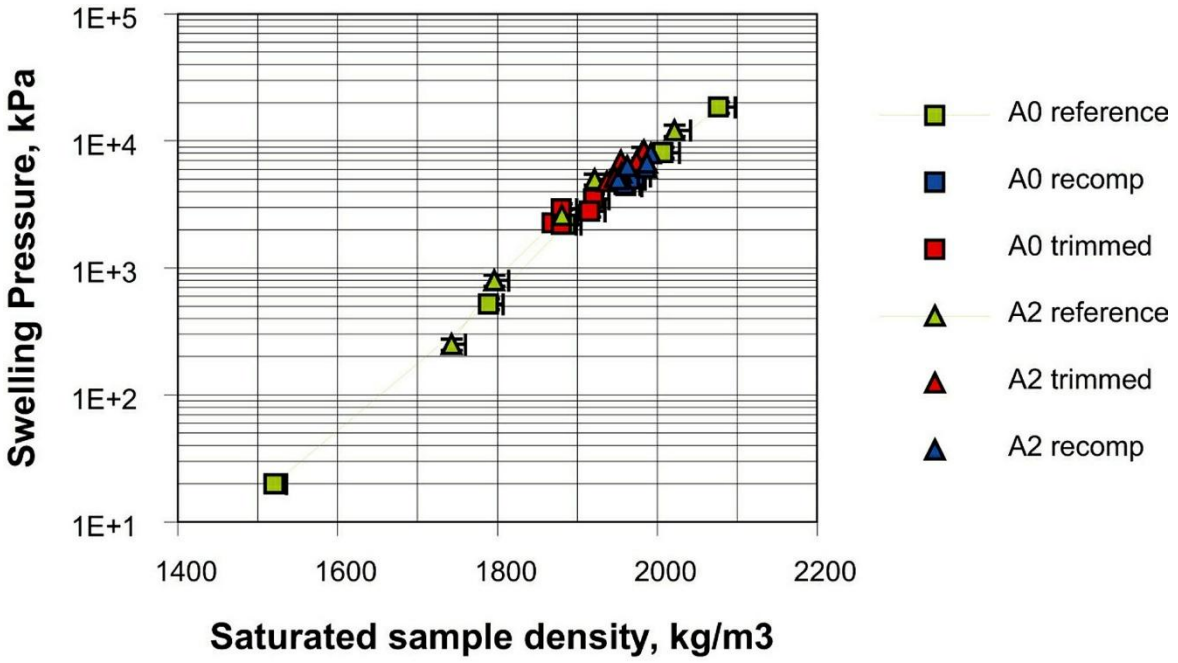

Figure 22: Measured swelling pressure results from the A2 parcel material compared with reference material and to the previous short term test material (A0) (Karnland et al 2009a).

The two test parcels S2 and A3 were installed in 1999 and dismantled after 20 years, in September 2019 (Svensson et al 2024). The temperature measurements show that the warmest section in test parcel S2 was between 700 and 1800 mm from the bottom. In this area the temperature has been between 70 and 90 °C close to the heater and between 60 and 70 °C closer to the rock. The warmest section in test parcel A3 was between 600 and 1700 mm from the bottom. In this area the temperature has been between 100 to 120 °C close to the heater and between 70 and 90 °C closer to the rock. The swelling pressure of samples was measured in two different laboratories using the same methodology as presented for A2 in the previous section. In order to remove effects from the type of interlayer cation and any salts in the sample, the Ca-exchanged samples with deionised water were selected to study details in the swelling pressure in LOT A3 and S2, while hydraulic conductivity was studied in detail using the 1 M $CaCl_2$ solution case, as it is the most demanding on the bentonite. As differences arising from cation exchange reactions otherwise easily can overshadow any differences in performance due to any potential mineralogical alterations. Swelling pressure data of samples taken from LOT A3 and LOT S2 are indistinguishable from the reference data (**Figure 23** and **Figure 24**). Hence, the swelling pressure performance was unaffected by the long term heating in the experiments.

In **Figure 25** the measured swelling pressure from LOT S-2 in equilibrium with the different solutions (LOT-water, 1M $CaCl_2$, DI-water) are shown. The results of specimens from the field experiment are shown together with reference lines. The reference lines are best fit lines of the results at equilibrium with LOT-water (dashed line), after ion-exchange and equilibrium with 1M $CaCl_2$ (dotted line) and after circulation with de-ionized water removing excess salt (solid line). Equilibrium with LOT-water was done both at stagnant and circulating conditions, but only small differences between the swelling pressure at these conditions were seen. In **Figure 26** the measured swelling pressure from LOT A3 in equilibrium with the different solutions (LOT-water, 1M CaCl2, DI-water) are shown.

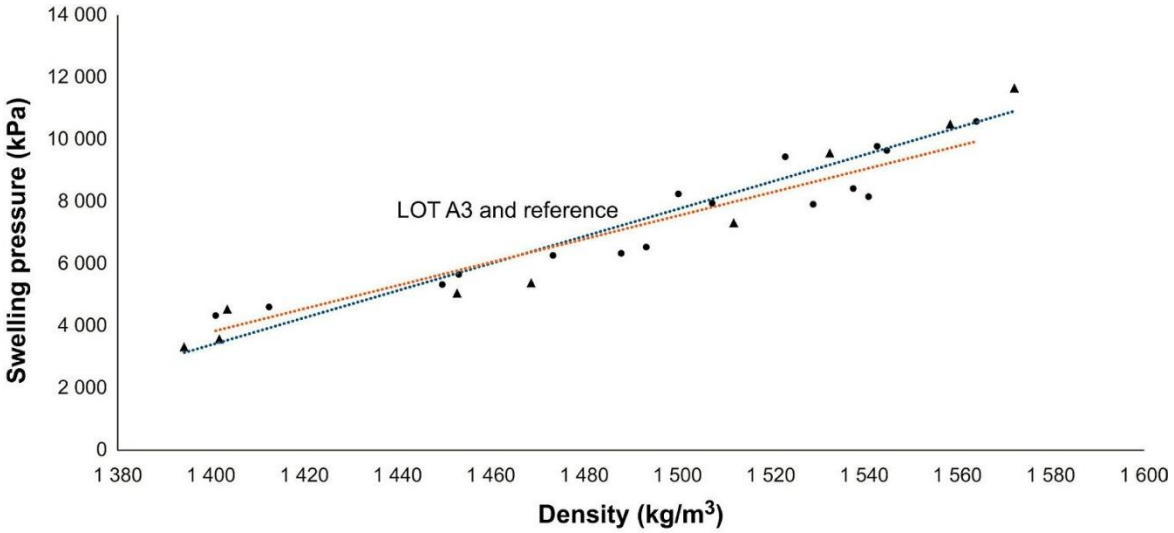

Figure 23: LOT A3 swelling pressure of Ca-exchanged samples after washing with deionised water. Circles = field experiment samples. Triangles = reference samples. Fittings are present as guides for the eyes (Svensson et al 2024).

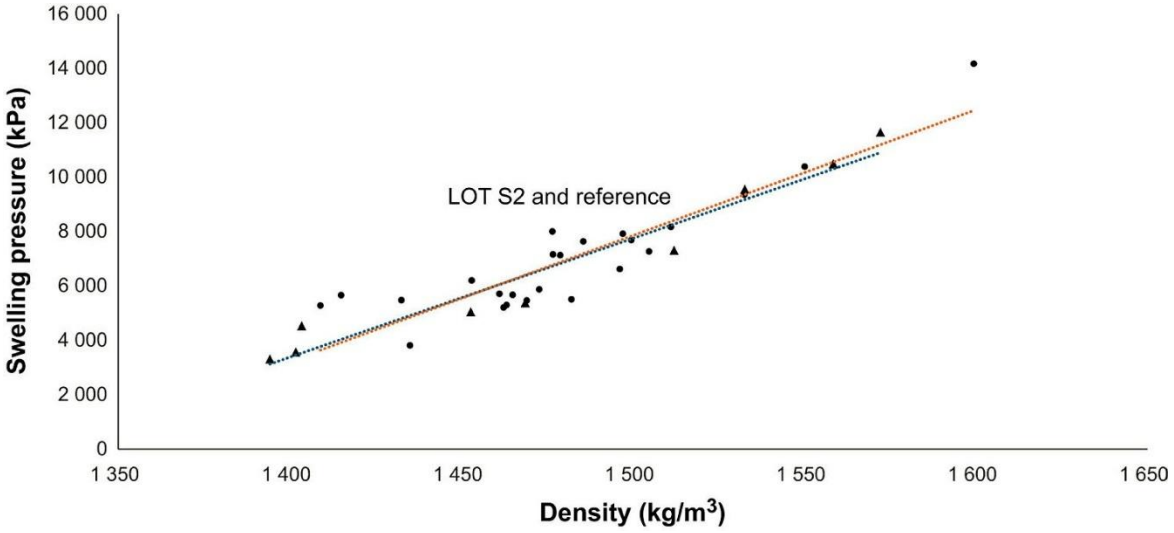

Figure 24: LOT S2 swelling pressure of Ca-exchanged samples after washing with deionised water. Circles = field experiment samples. Triangles = reference samples. Fittings are present as guides for the eyes (Svensson et al 2024).

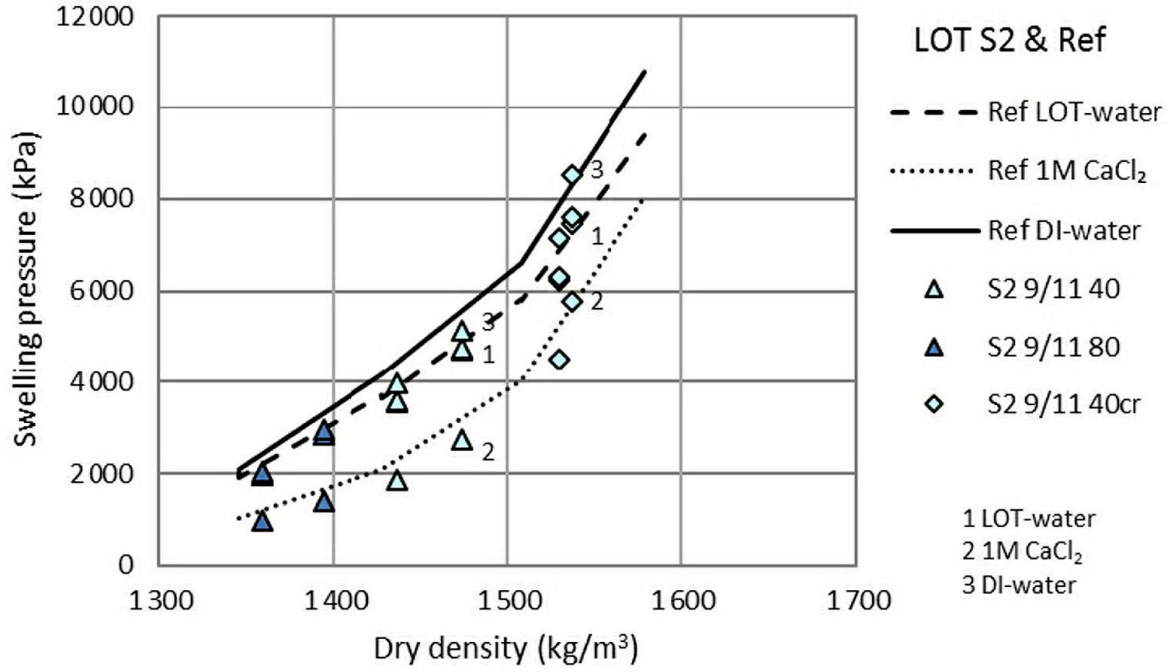

Figure 25: Measured swelling pressure of specimens sampled from LOT S2. Results from different conditions (1–3), in equilibrium with 1) LOT-water, 2) 1M $CaCl_2$, and 3) de-ionized water. Results of drilled specimens (triangles) and crushed/compacted specimens (diamonds) are shown with reference results (black markers). Results from reference tests at the different conditions are shown with lines (dashed, dotted, solid) (Svensson et al 2024).

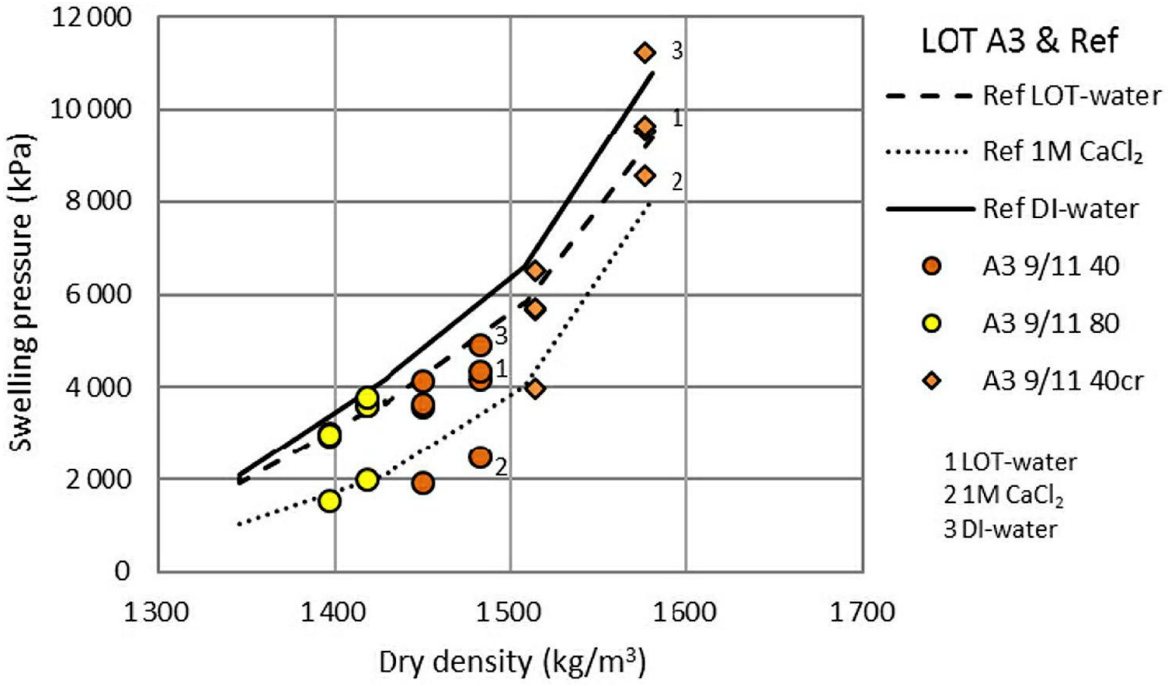

Figure 26: Measured swelling pressure of specimens sampled from LOT A3. Results from different conditions (1–3), in equilibrium with 1) LOT-water, 2) 1M $CaCl_2$, and 3) de-ionized water. Results of drilled specimens (circles) and crushed/compacted specimens (diamonds) are shown with reference results (black markers). Results

from reference tests at the different conditions are shown with lines (dashed, dotted, solid) (Svensson et al 2024).

ABM

Expanding the knowledge base on alternative buffer materials is essential for optimizing safety, availability, and cost-effectiveness. Consequently, the Alternative Buffer Material (ABM) field experiment was initiated at the Äspö Hard Rock Laboratory in 2006. The main objectives of the ABM project were to characterize the mineralogical content of different clays and identify any variations in behavior or long-term stability after exposure to field conditions. The ABM 1–3 test series was installed in 2006. The experiment comprised three medium-scale test packages, each consisting of a central steel tube with heaters and a buffer of compacted clay. Eleven different clays were selected for the buffers to investigate the effects of smectite content, interlayer cations, and overall iron content. Additionally, bentonite pellets with and without additional quartz were tested. Test package 1 (ABM1) had a maximum temperature of ~130 °C and was retrieved in 2009, and the status of the material investigations was reported by Svensson et al. in 2011. Test package 2 (ABM2) was retrieved in 2013. A second test series, ABM 45, was installed in 2012. This new test series also included three test packages with the same design principle as the first test series, but some of the materials used in the first series were replaced with others. Test package 5 (ABM5) was retrieved in 2017.Test package 3, 4 and 6 were retrieved in 2025, but is still not analysed.

In ABM 1 swelling pressure measurements have been made on three materials: MX-80, Asha and Deponit CAN (Svensson et al 2011). Totally twenty-three tests were made (ten on the reference materials and thirteen on specimens taken from the blocks in test package. The methodology was the same as for the LOT test. The results are presented in Figure 6-14 to 6-16., where the swelling pressure is plotted versus the dry density of each sample.

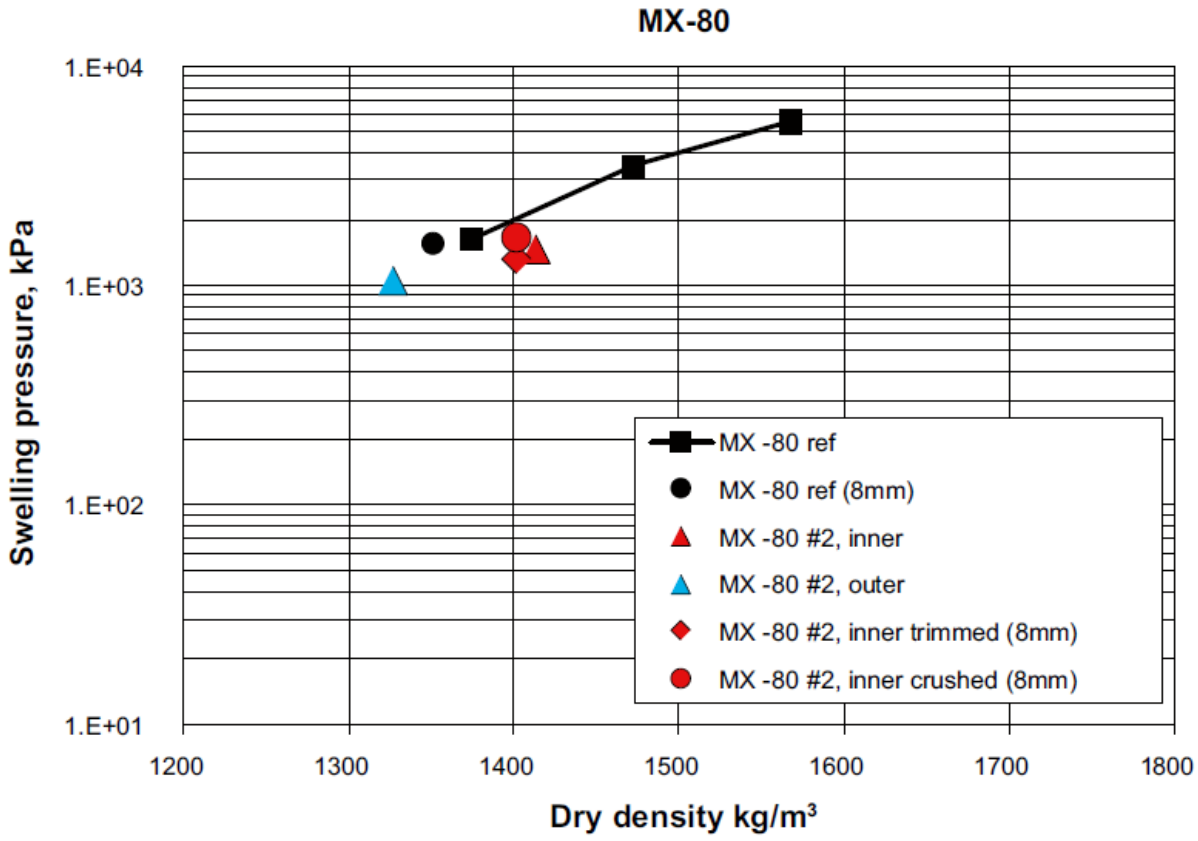

Figure 27: Swelling pressure plotted versus dry density for the MX-80 samples in ABM 1 (Svensson et al 2011).

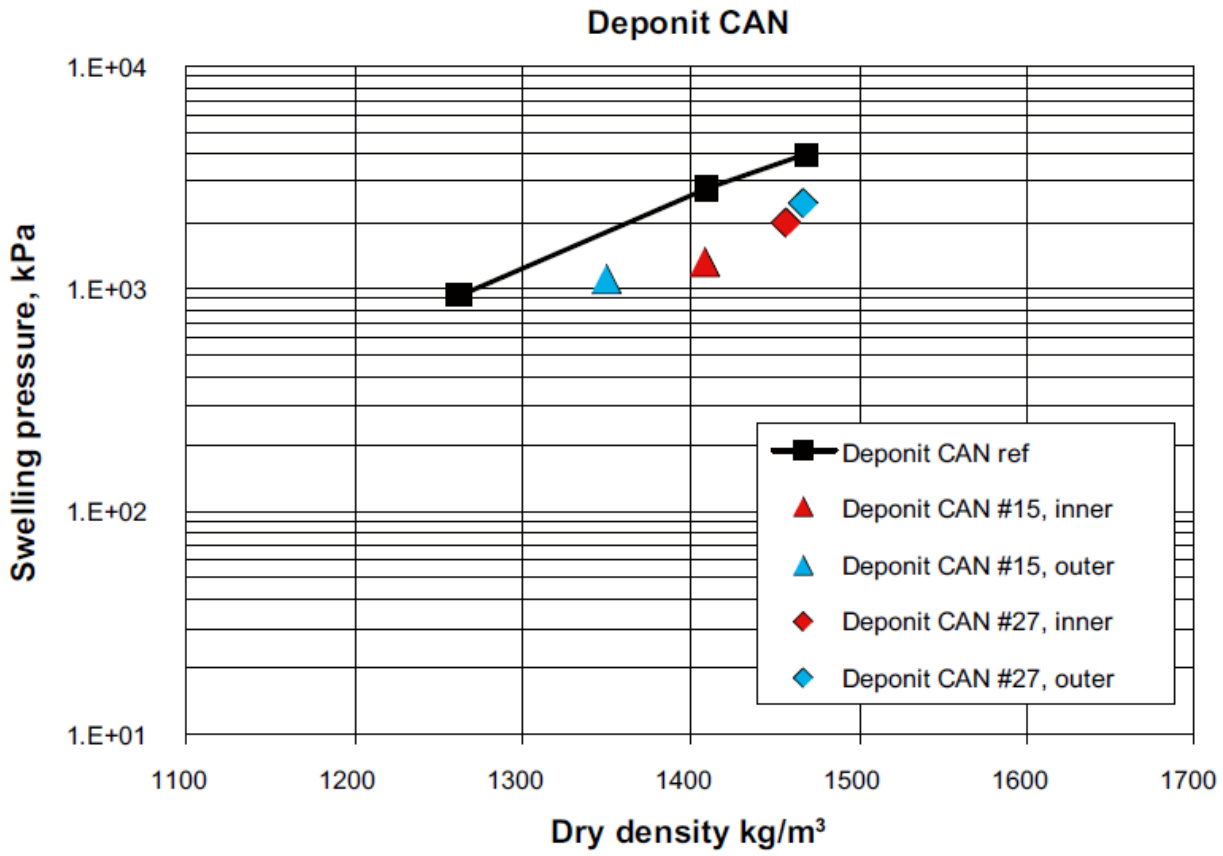

Figure 28: Swelling pressure plotted versus dry density for the Deponit CAN samples in ABM 1 (Svensson et al 2011).

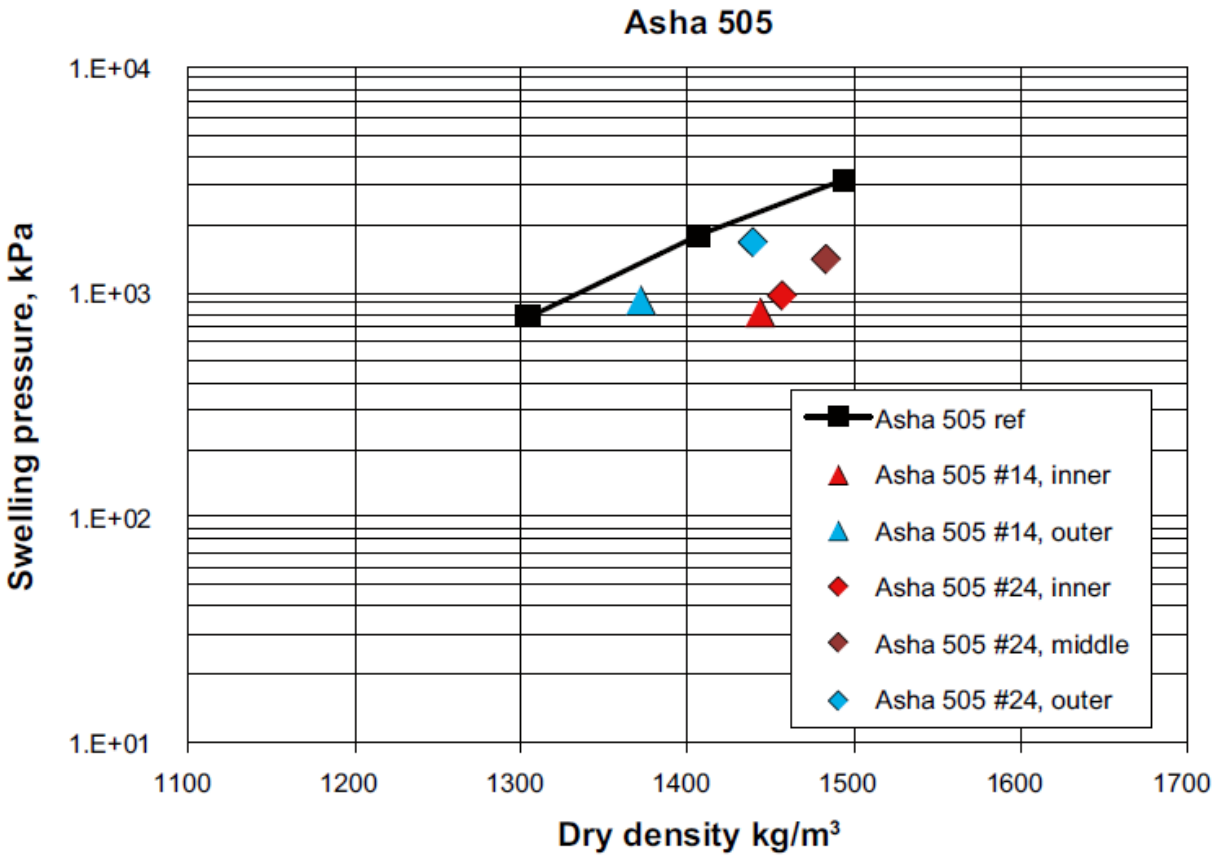

Figure 29: Swelling pressure plotted versus dry density for the Asha 505 samples in ABM 1 (Svensson et al 2011).

The results showed a significant difference in swelling pressure between test parcel material and reference material for two of the investigated materials, Asha 505 and Deponit CAN. The measured swelling pressure for these two materials is lower for material taken from the test parcel. There is also a tendency that the decrease is greater for samples taken from the hottest part i.e. close to the heater. One possible explanation for the registered decrease in swelling pressure is, that there has been a large redistribution of cations in the test package, and this has influenced the physical properties of the materials.

ABM 5 was kept at a relatively low temperature for a long time due to issues with the water pressure control in the test (Svensson et al 2023). After around 3 years the heater power was increased and the temperature increased to ~250 C at the surface of the heater pipe. The measured temperature for block 15 in the middle of the test is shown in **Figure 30**.

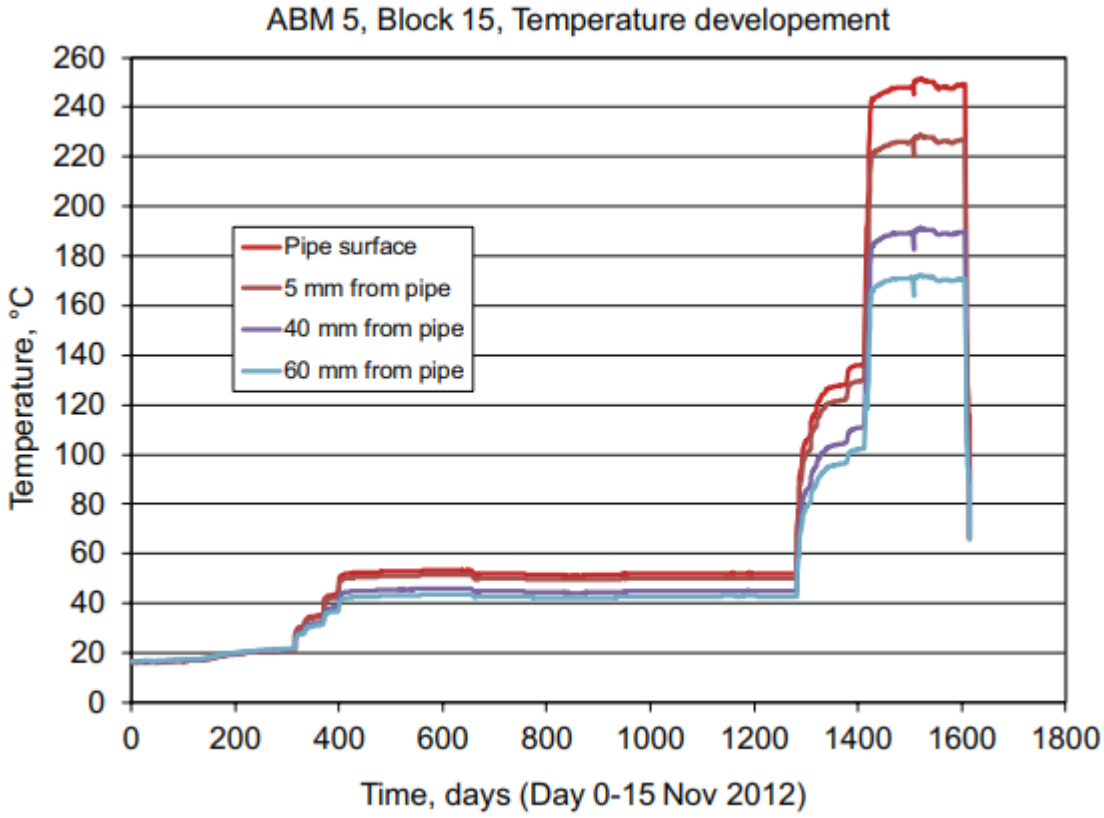

Figure 30: Temperature measurements in block no. 15 plotted vs. time (Svensson et al 2023).

The swelling pressure was measured in a series together with hydraulic conductivity in several different chemical conditions. First with deionised water, then with salt solution (1 M CaCl2), and then again with deionised water. By looking on the last step one gets the swelling pressure with deionised water. Hence one can compare the material from the experiment with the reference clay and at the same time excluding effects from cation exchange and salt accumulation which is ideal conditions for finding smectite degradation. In Calcigel (**Figure 31**) the densities ended up a little bit low for ideal comparison, they suggest a possible small increase in swelling pressure in the samples from ABM5 compared to the reference samples. However, the hydraulic conductivity showed a possible increase. Typically, when the swelling pressure performance increase due to increased smectite content the hydraulic conductivity should decrease. Most likely the explanation for this is that the experimental uncertainties increased at the lower densities used, and the difference in behaviour is far from certain. In Asha505 (**Figure 32**) the swelling pressure was the same in both ABM5 samples and references. In some samples from the ABM5 experiment at low densities the hydraulic conductivity increased, like in the calcigel case. In DepCAN (**Figure 33**) and in MX-80 (**Figure 34**) no significant change could be seen between ABM5 samples and reference samples either in swelling pressure or hydraulic conductivity. Summary: At the lowest tested densities possibly, there were some changes in performance between samples from ABM5 and reference materials, most likely this was due to the experimental difficulties at the low densities. At the higher densities (the target densities) no change in performance was observed. This is a clear difference to some of the observations from ABM1 and is more in line with the results from LOT.

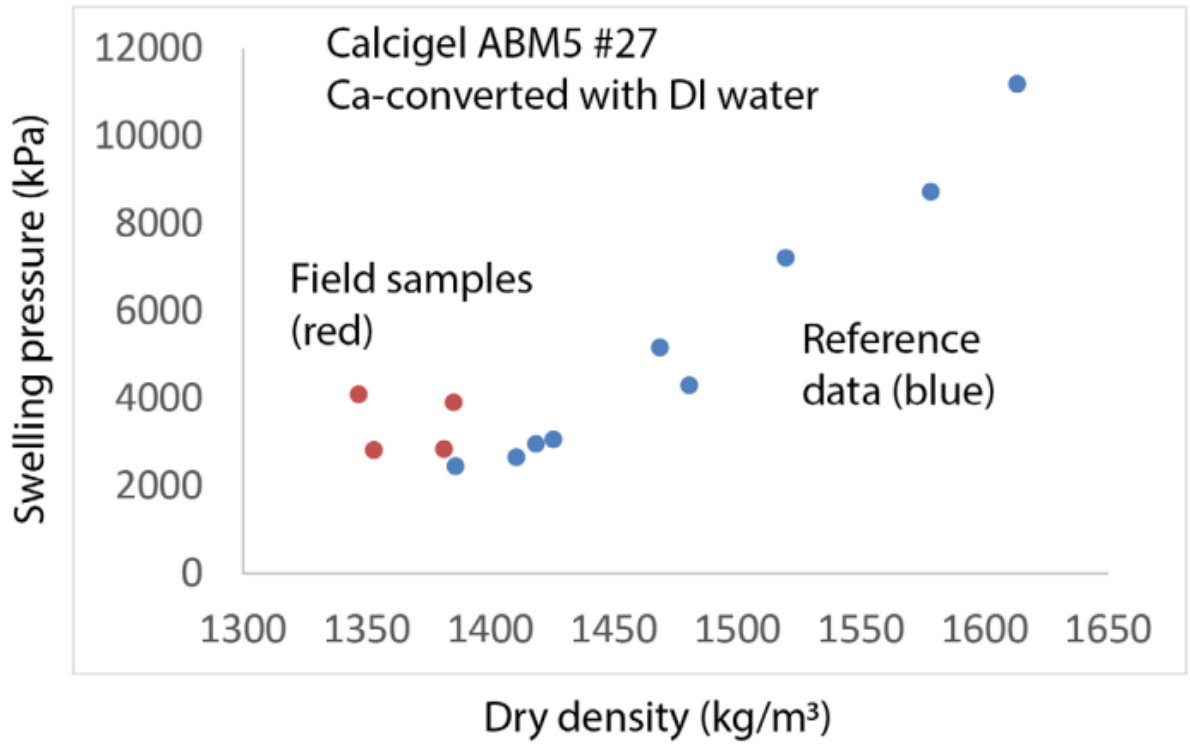

Figure 31: ABM5 Calcigel #27 samples compared to reference samples. Swelling pressure after Ca-conversion in DI water (Svensson et al 2023).

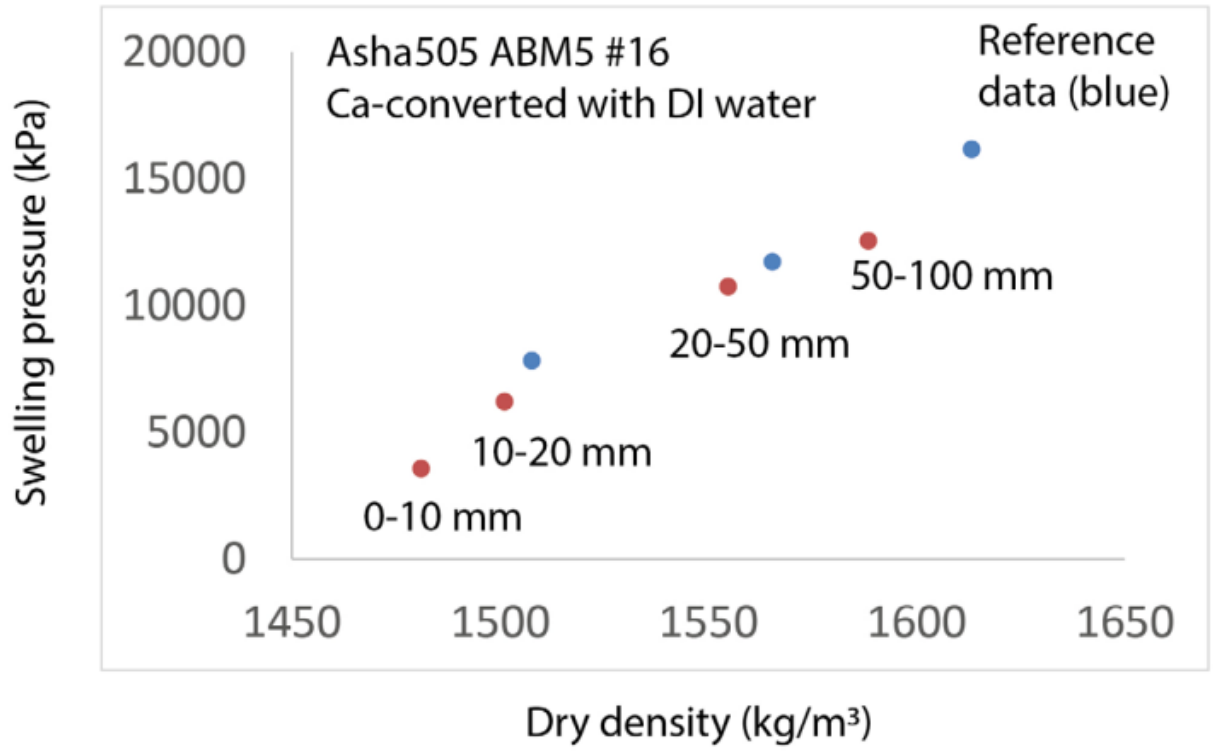

Figure 32: ABM5 Asha505 #16 samples compared to reference samples. Swelling pressure after Ca-conversion in DI water (Svensson et al 2023).

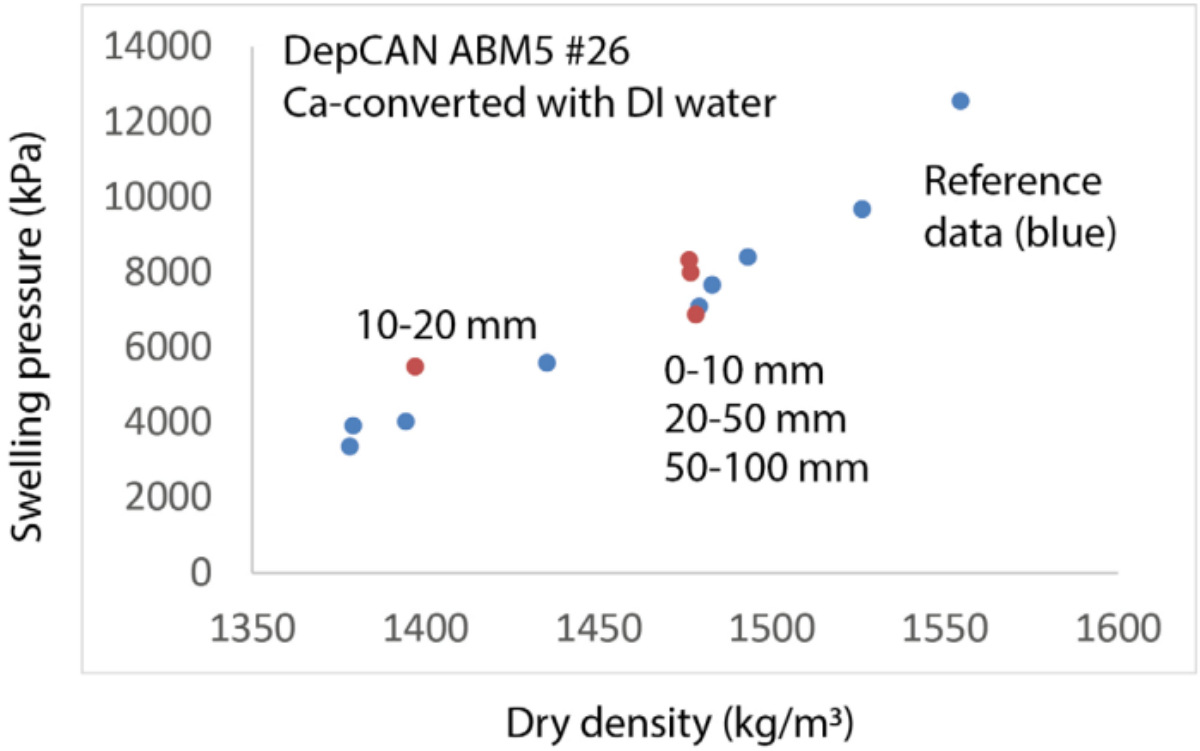

Figure 33: ABM5 DepCAN #26 samples compared to reference samples. (Swelling pressure after Ca-conversion in DI water (Svensson et al 2023).

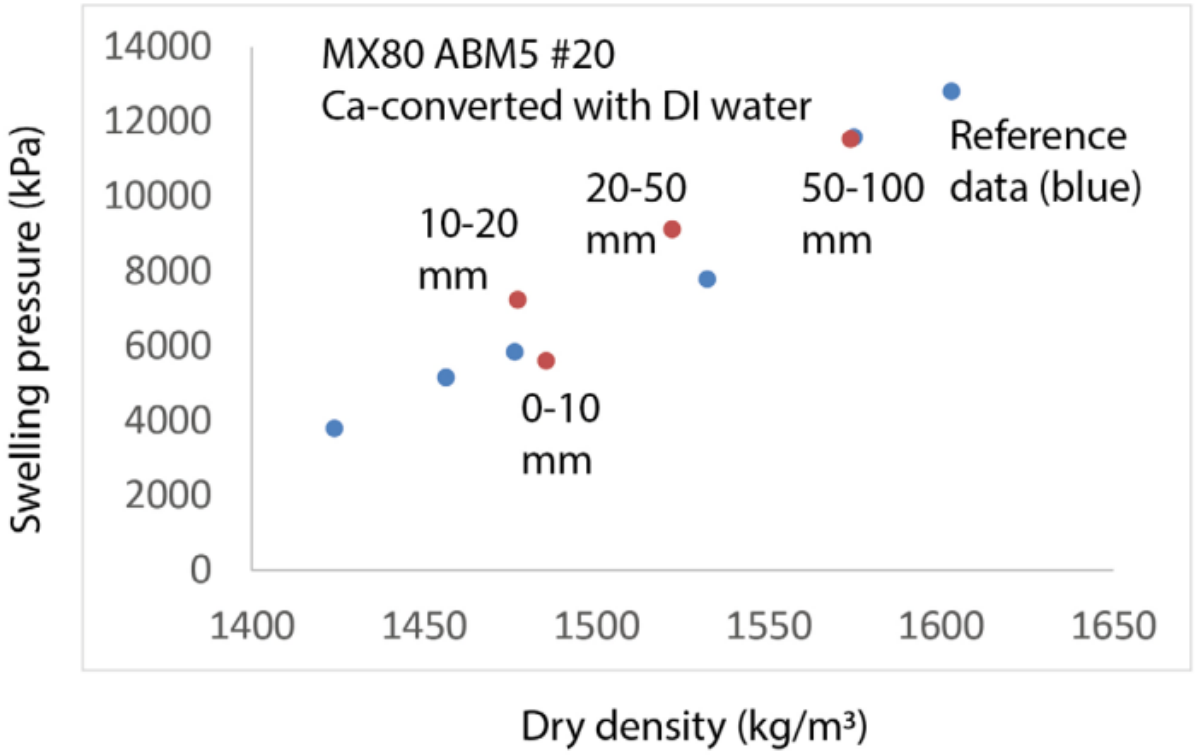

Figure 34: ABM5 MX-80 #20 samples compared to reference samples. Swelling pressure after Ca-conversion in DI water (Svensson et al 2023).

Prototype Repository

The Prototype Repository field test at Äspö Hard Rock Laboratory is a full-scale experiment simulating conditions relevant for the Swedish KBS-3 concept for final disposal of high-level radioactive waste. The Prototype gallery consisted of six deposition holes and was divided into two sections, containing four and two holes, respectively. Each deposition hole had a full-scale buffer of compacted bentonite (MX-80) surrounding a copper canister equipped with heaters to simulate the heat generation from radioactive waste. the outer section (deposition holes 5 and 6), was retrieved in 2010–2011 after about 8 years of hydrothermal exposure, aim at improving the understanding of the hydro-mechanical and chemical behavior of bentonite buffers at temperatures around 100°C during the water saturation transient. The inner section was retrieved 2024-2025 and the investigations of the material from that part is still ongoing.

The acid-proof stainless steel test equipment used for hydraulic conductivity and swelling pressure determinations is shown in **Figure 35** (Olsson et al 2013). One series of tests from each deposition hole, 5 and 6 respectively, was run. In every series three types of specimens were tested; reference specimens and specimens from the field experiment prepared in two different ways:

- Material saved at the block production was compacted aiming at the saturated densities 1900, 1950, 2000, 2050, 2100 and 2150 kg/m^3 at full water saturation (references). These densities correspond to dry densities of 1,410, 1,480, 1,560, 1,640, 1,720 and 1,800 kg/m3 respectively.
- Specimens were drilled and trimmed to fit the sample holders, thus having a density close to the field value.
- Block samples were air-dried and ground to a grain size similar to the original MX-80 powder and re-compacted to a density at saturation of 2,000 kg/m3 which corresponds to a dry density of 1,560 kg/m3. The purpose of this treatment of the material is to investigate whether potential differences between the field-exposed material and the reference samples are related to changes in the bentonite or to changes in the structure in the buffer material (e.g. precipitates).

The specimens were saturated or re-saturated after preparation by introducing water to the bottom and top side simultaneously. Water was added after evacuation of air from filters and tubes by a vacuum pump. Groundwater from the Prototype test site was used for all specimens.

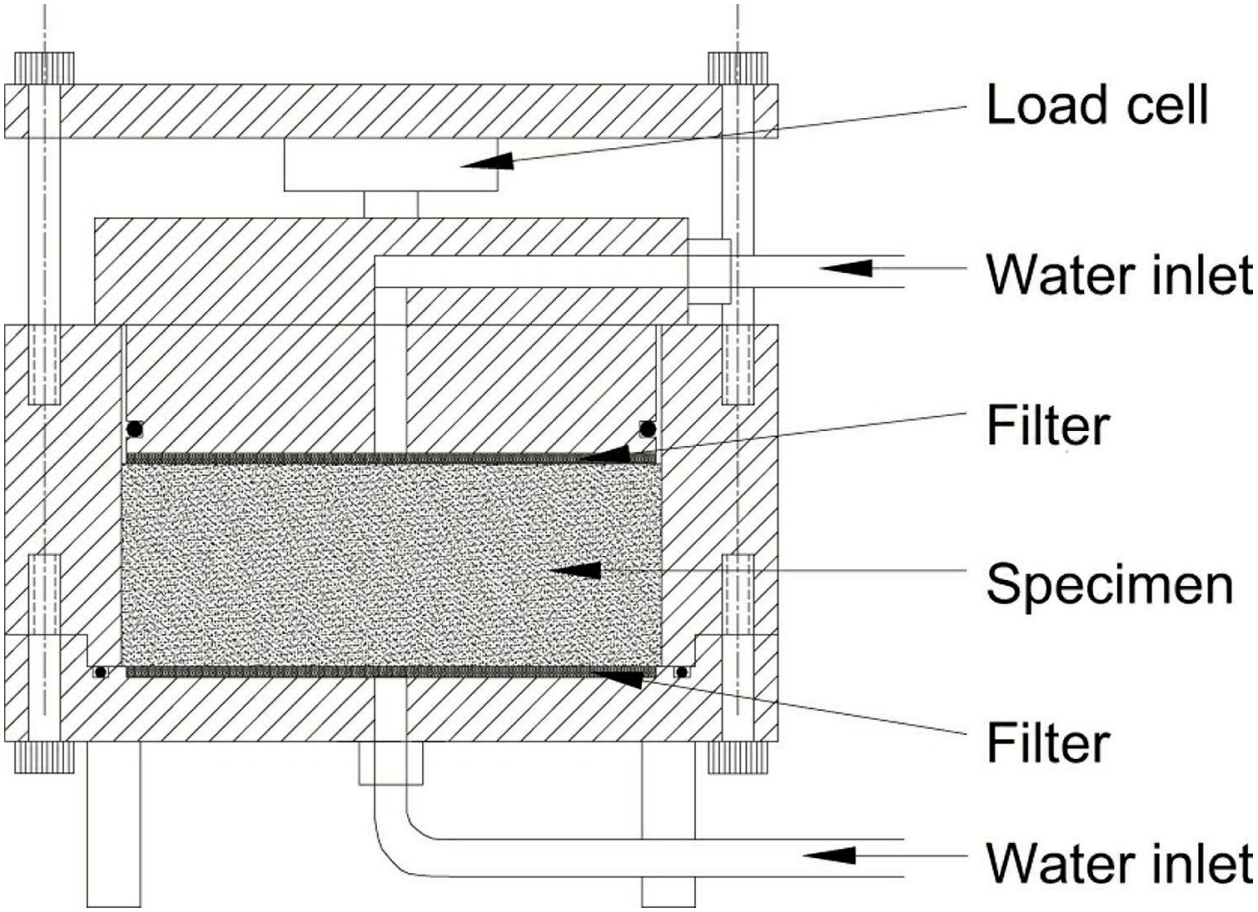

Figure 35: A schematic drawing of the swelling pressure device (Olsson et al 2013).

The results from measurements of swelling pressure of samples from deposition hole 5 and 6 are plotted as a function of dry density in **Figure 36** and **Figure 37**. In the diagrams the green and red colors denote deposition hole 5 and 6, respectively. In the figures diamonds and squares indicate drilled specimens and triangles and circles represent ground and compacted samples. The references are indicated with black crosses.

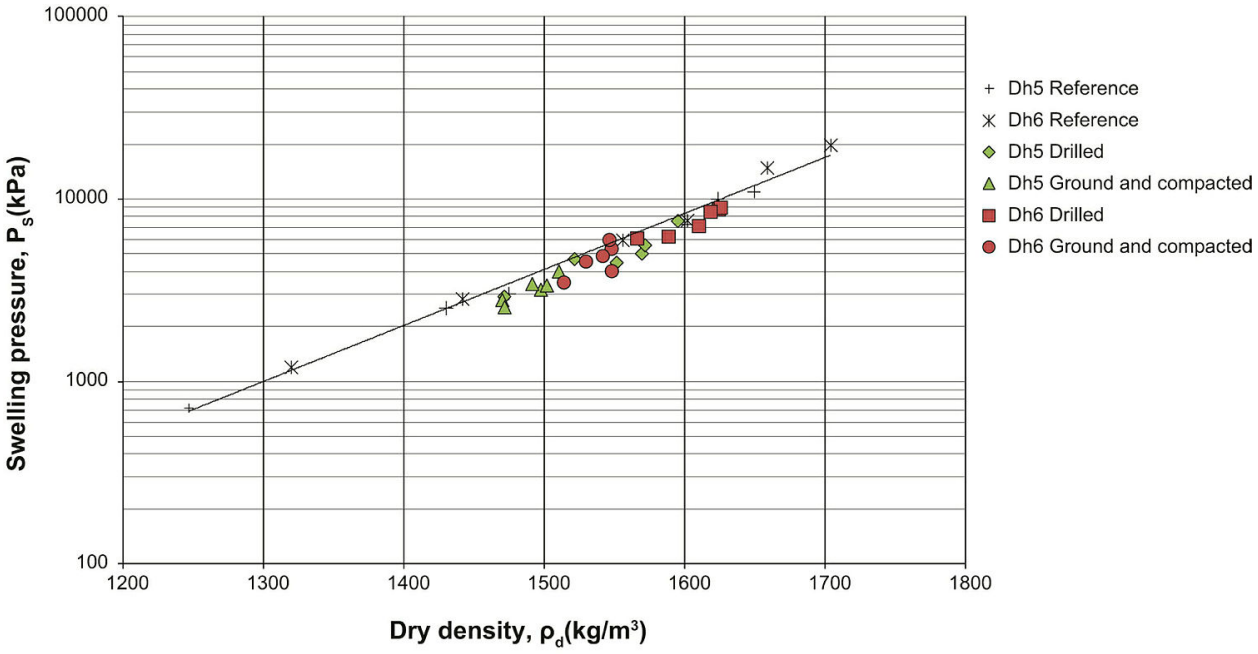

Figure 36: The determined swelling pressure as a function of the dry density of samples from deposition holes 5 and 6. Black points denote results from measurements made on reference samples (Olsson et al 2013).

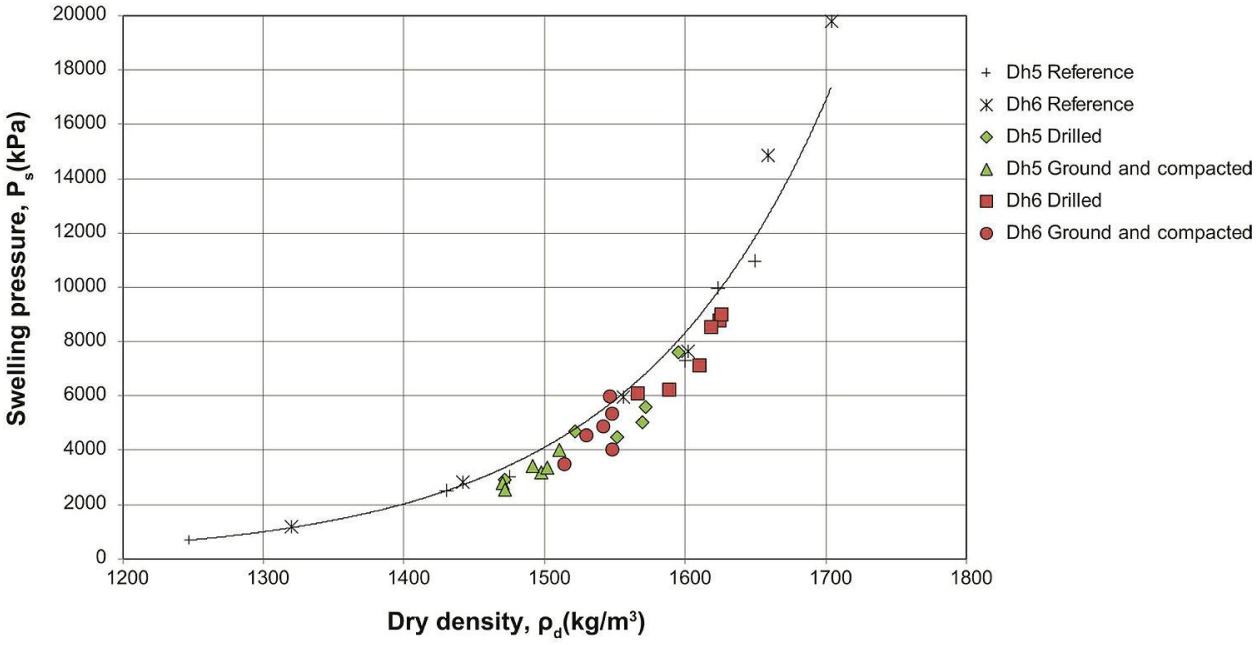

Figure 37: Results as in **Figure 36** but with a linear scale on the y axis (Olsson et al 2013).

There are no large variations in swelling pressure between the reference specimens and the specimens of field-exposed material although there is a small tendency that the swelling pressures of the field-exposed material are somewhat lower, i.e. all the green diamonds and the red squares in **Figure 36** and **Figure 37** plot under the solid line representing the swelling pressure of the reference specimens.

Field test summary

Most results from long-term field tests show no or very little difference in swelling pressure between field samples and reference samples. There are however a few samples where a decrease in swelling pressure has been observed. The reason for this decrease is unclear.

2.3 Posiva

Posiva has set maximum temperature limit of 100 °C for buffer and expected thermal gradient in buffer is at highest expected to be from 100 °C at canister contact to 70 °C at host rock contact (from 95 °C to 65 °C in thermal dimensioning that contains a 5 °C safety margin, see **Figure 38**)

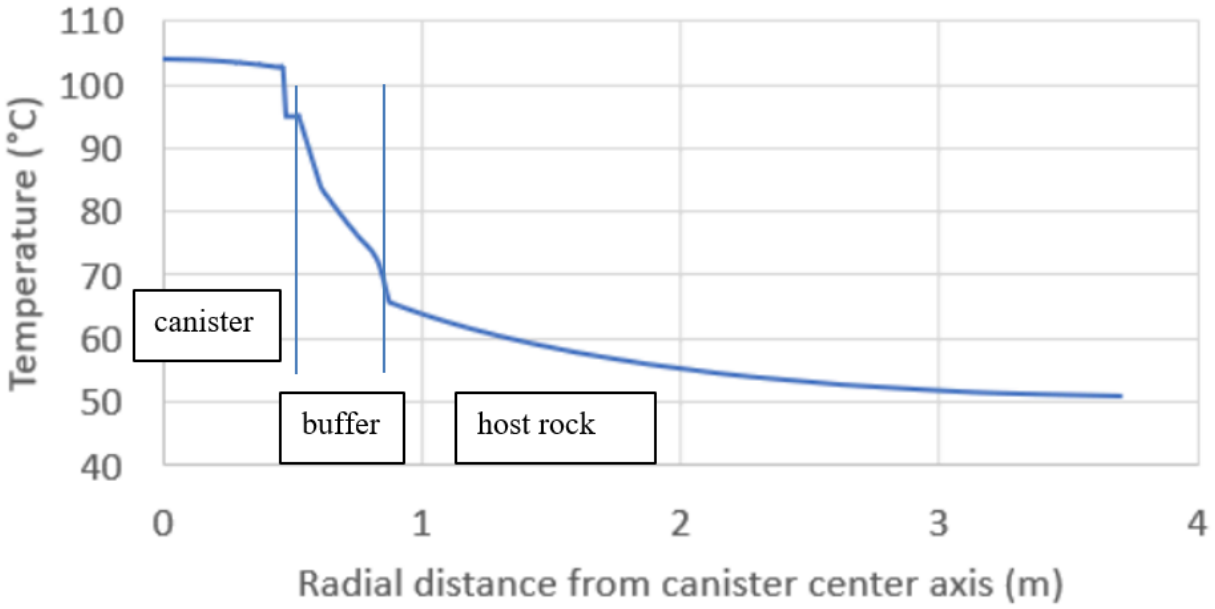

Figure 38: Expected radial temperature profile, bentonite buffer marked inside vertical lines

Posiva has done some bentonite tests in elevated temperatures. One such test series is "Empirical Assessment of Block-Pellet Density Homogenization", where bentonite homogenization tests were performed for a test setup containing initial inhomogeneity from being composed of blocks and pellets. The experiment was a multi-factor experiment where the effect of 9 different factors, including bentonite material (4 different bentonites) and temperature (room temperature, ~25 °C and 90 °C in heated chamber) was assessed on axial swelling pressure and final homogeneity of the system. Test cells were given two years to homogenize and total of 19 small scale tests + 1 dummy test with sand were carried out.

While focus of the testing was in the final dry density profile, some interesting results related to swelling pressure were also seen. The swelling pressure was on average lower in high temperature cells (3.1 MPa) compared to room temperature cells (4.5 MPa). Moreover, some of the high temperature tests showed a decrease in swelling pressure in time (see **Figure 39** and **Figure 40**).

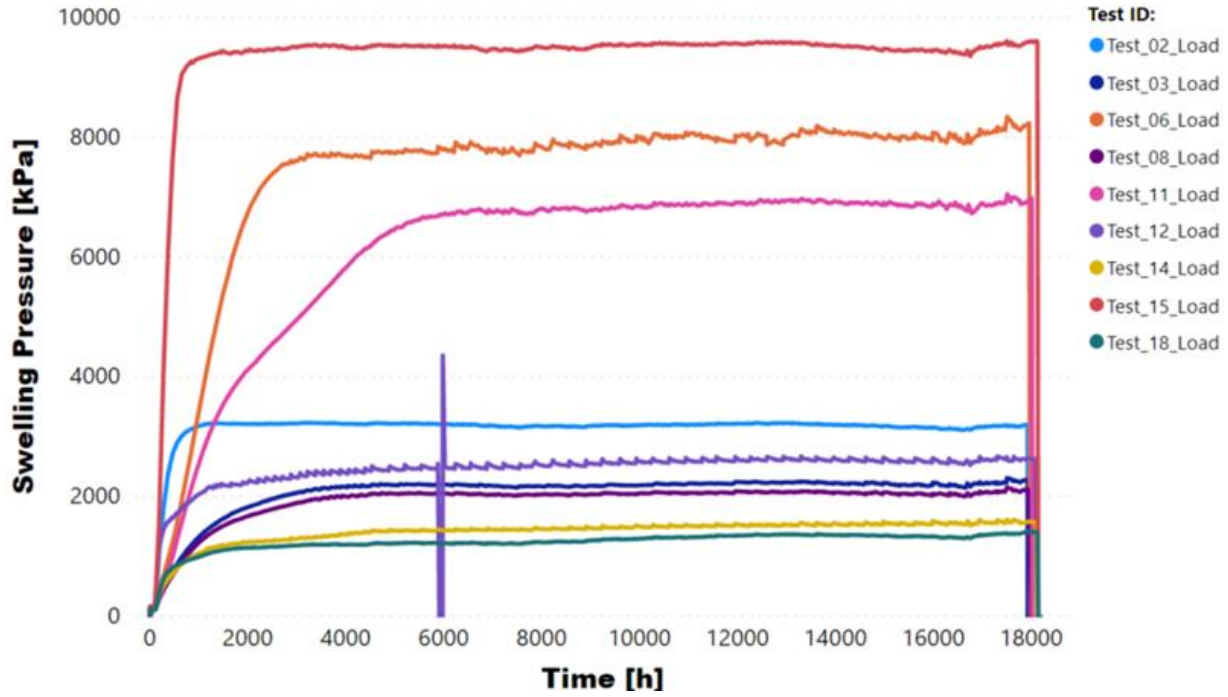

Figure 39: Swelling pressure development of room temperature cells.

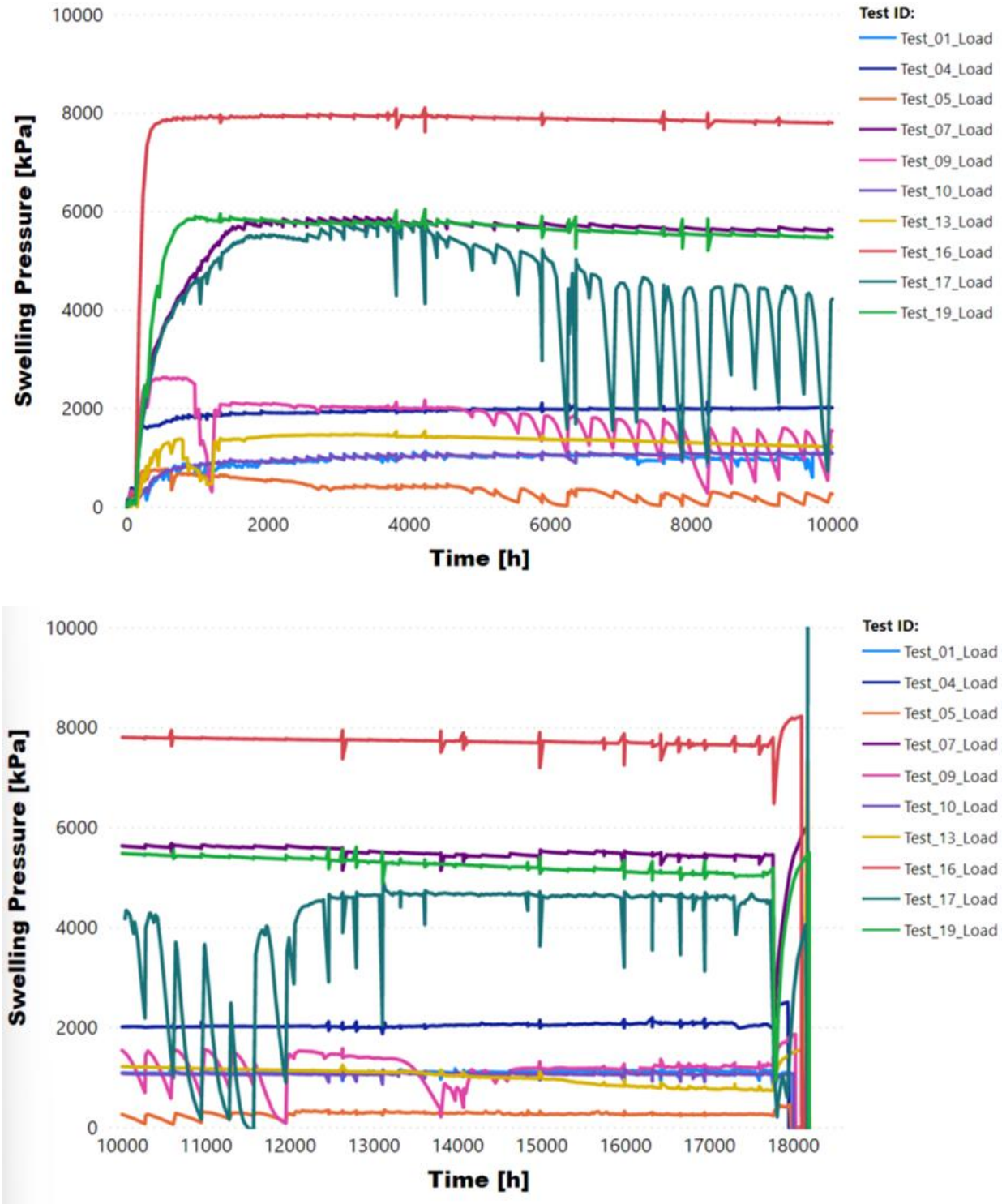

Figure 40: Swelling pressure development of high temperature cells.

However, similar decrease in swelling pressure was also seen in the dummy cell filled with sand. Dummy cell was tightened to have pressure of ~2.1MPa prior to turning the heating on. During the two years of heating the pressure lowered to 1.6 MPa but increased to 1.9 MPa during cooling in room temperature (see **Figure 41**). Similar increase was seen for many bentonite cells as well.

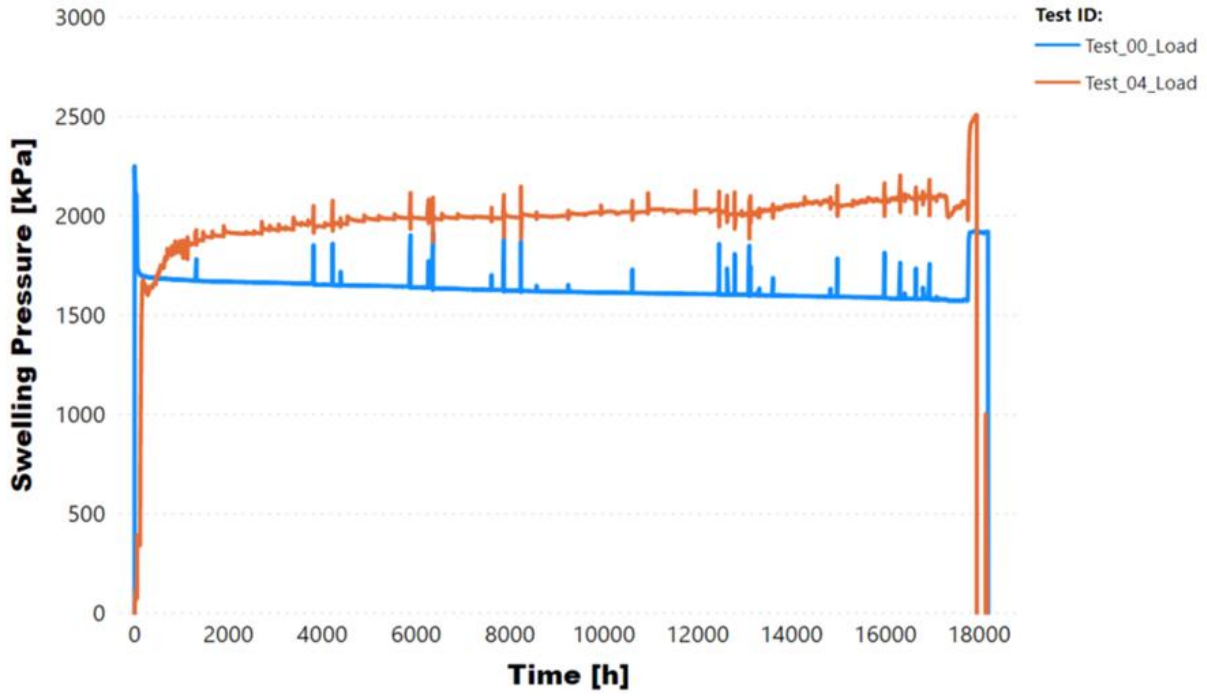

Figure 41: Swelling pressure development of high temperature dummy cell (00) and bentonite cell (04).

Because decrease of pressure in time is seen in dummy cell and test cells, it is difficult to say if it is caused by the test setup. However, swelling pressures were on average lower in high temperature tests as well.

Another potential example of elevated temperatures on buffer behaviour was seen in a heated experiment where piping channel formation was studied with a transparent test system. These test setups were built in transparent 27 cm wide and 80 cm tall test cylinders and were composed of blocks and pellets. The core of blocks was heated to 65 °C and outside and inflowing water to 50 °C. Water was pumped inside the cell from the inlet located near the bottom of the cylinder and collected from outlet ~70 cm above the inlet (see **Figure 42**).

Figure 42: Piping erosion experiment.

A total of two experiments were done and in the first experiment a very wide erosion channel was seen on the surface of the test cell. Typically, the erosion channels have been 5 mm in width in similar room temperature experiments, but channel seen in experiment 1 was 2-3 cm in width. However, experiment 2 done with the same parameters only had a 5 mm erosion channel. In any case, heated bentonite or heated water might have affected the bentonite mechanical behaviour.

2.4 NWS

The siting policy for a UK Geological Disposal Facility (GDF) incorporates a consent-based approach, with Nuclear Waste Services (NWS) working in partnership with potential communities to determine if hosting a GDF is right for them. A GDF will only be built where both a willing community and a suitable site can be demonstrated [4, 5]. At the time of writing (November 2025), NWS is working with two Community Partnerships in the UK (Mid Copeland and South Copeland in Cumberland).

NWS is evaluating GDF construction, operation and long-term behaviour in the potential host rocks present in these Community Partnership areas, focussing initially on disposal concepts developed by other waste management organisations and their possible adaptation to UK-specific conditions. These disposal concepts are captured in NWS' 2016 generic Disposal System Safety Case [6]. In some of these concepts, bentonite-based materials are used as a buffer around High Heat Generating Wastes (e.g., spent fuel) containers because of bentonite's low hydraulic conductivity, self-sealing capacity, ability to minimise microbial activity and for its potential durability in the environmental conditions expected within a GDF and host rock [7].

As the programme to deliver a GDF progresses, NWS will optimise the design of the facility. One aspect of the optimisation process will consider the GDF 'footprint' (plan area), noting that a smaller footprint might require less site investigation and engineered barrier materials, and could therefore be cheaper to implement with a lower environmental impact. Currently, NWS envisages a thermal limit on the bentonite buffer to protect its safety functions. However, increasing this thermal limit could allow the GDF footprint to be reduced by minimising the spacing between waste containers. To do this, NWS needs a thorough understanding of the coupled thermal-hydraulic-mechanical-chemical processes occurring in bentonite at elevated temperatures (>100˚C).

Preliminary investigations on the behaviour of bentonite at elevated temperatures were carried out by the British Geological Survey (BGS), as part of the *Safe Barriers* project funded by the UK Engineering and Physical Sciences Research Council (EPSRC). In this project the BGS investigated how cycling temperatures from room temperature up to 200˚C and back influences the hydro-mechanical properties of bentonite [8]. Sub-samples of Wyoming bentonite blocks (VOLCLAY MX-80, hereafter referred to as MX-80) compacted to 1,560 kg/m^3 dry density were tested. The main purpose was to evaluate the impact of temperature variation with time on bentonite permeability. Information was also obtained on the total stress, swelling pressure and pore pressure during heating / cooling cycles. The main conclusion was that permeability was not significantly impacted by increasing temperature. However, one constant volume test (CVRF-2) showed that when temperatures reached 150˚C, the total stress (and therefore swelling pressure) continuously reduced over the duration of the test. Increasing the temperature to 200˚C resulted in further total stress reduction, although BGS indicated that this could be caused by the experiment exceeding the boiling point of water at the lower water pressure applied at the backpressure end (1 MPa), affecting the water present in 1/5 of the bentonite sample, and could represent an experimental artefact.

To develop NWS' understanding of bentonite behaviour at elevated temperatures, NWS co-funded BGS to participate in the EURAD HITEC Work Package. BGS explored the influence of temperature between 100 and 200˚C on swelling pressure and permeability of MX-80 bentonite samples, testing fully constrained samples as well as samples that could swell into voids [9]. The swelling pressure was measured for fully constrained bentonite samples in constant volume cells of 60 mm internal diameter and 120 mm length. A 4.5 MPa pressure was applied at both ends of the samples to be comparable to in-situ pore pressures expected in the Swedish (SKB's) GDF. The high pore pressure also increases the boiling point of water above 200˚C, i.e. water in the

bentonite remains liquid in the experiments. The MX-80 bentonite samples were compacted to dry densities of 1,300, 1,500 and 1,700 kg/m^3. The results of these tests are shown in Error! Reference source not found., which show that swelling pressure is significantly higher at 1,700 kg/m^3 compared to 1,300 kg/m^3, in line with expected behaviour of bentonite when at room temperature. There is also a clear dry density dependence on the evolution of swelling pressure over time. The swelling pressure remains constant at 100˚C and 150˚C and slightly increases at 175˚C at 1,300 kg/m^3, however it decreases over time at 1,700 kg/m^3, with the swelling pressure degradation rate increasing with temperature.

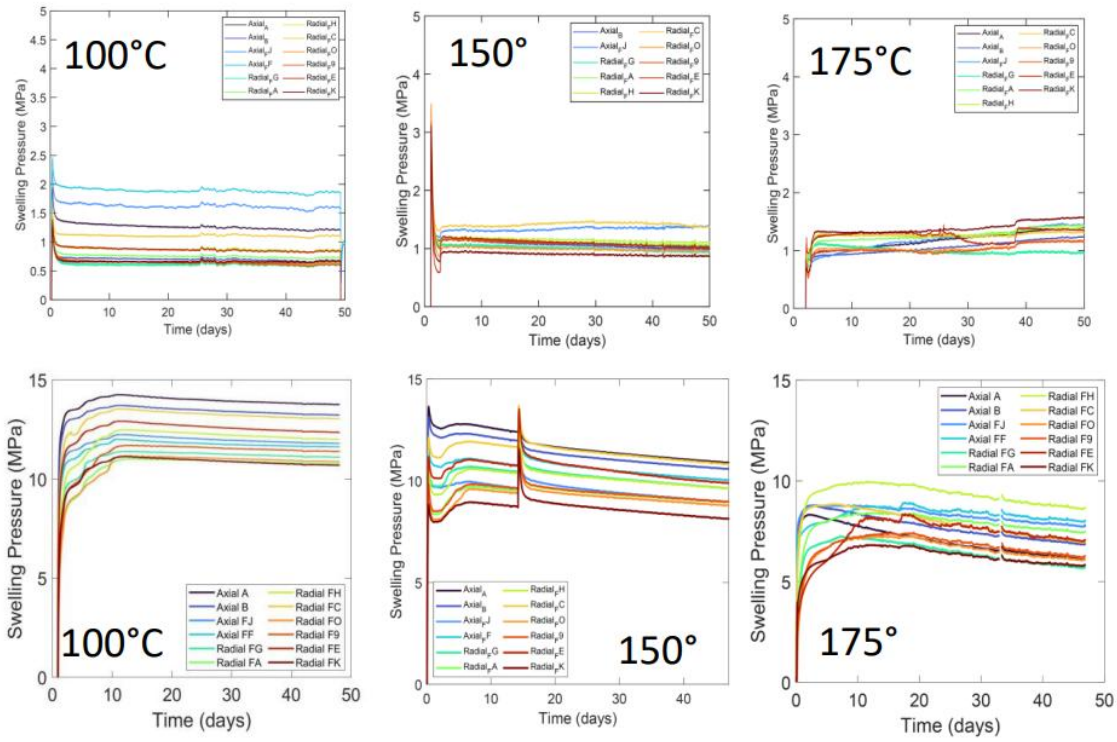

Figure 43: Swelling pressure evolution of MX-80 bentonite samples with dry density of (top row) 1,300 kg/m3 and (bottom row) 1,700 kg/m

BGS also monitored stress development during the permeability tests in constant volume radial flow cells, where temperature was cycled between 100˚C and 200˚C in 50˚C steps. The MX-80 samples were compacted to dry densities of 1,560 kg/m^3 (to provide comparison to [8]) and 1,700 kg/m^3. A 2 MPa water pressure was applied at both ends during hydration. The pressure was subsequently increased to 4 MPa at the injection end of the sample to apply a hydraulic gradient during permeability testing. The increased pore pressure at the back end prevented water boiling compared to the experiments carried out in the *Safe Barriers* project. The results from these tests showed a similar trend of reducing total stress (and therefore reducing swelling pressure) over time, with the rate of degradation in swelling pressure increasing with temperature. This is illustrated for the 1,560 kg/m^3 dry density sample in **Figure 44**. Permeability was observed to slightly increase. However, this is not expected to impact the performance of the buffer (permeability measured remained within 1E^{-21} m^2), in agreement with earlier investigations [8].

Overall, the experimental results demonstrate that increasing temperature has an observable impact on the swelling pressure generated by MX-80 bentonite, and further investigation is required to elucidate the responsible mechanisms.

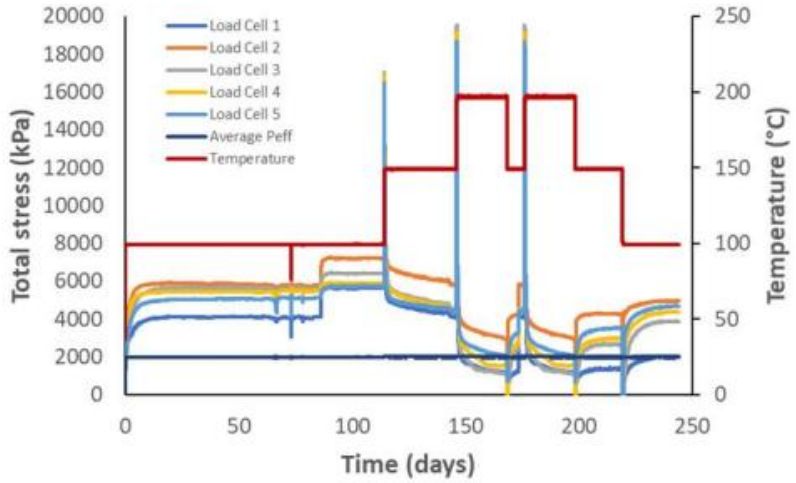

Figure 44: Total stress evolution for a 1,560 kg/m3 MX-80 bentonite sample. Temperature cycled in 50°C steps between 100 and 200°C

2.5 NWMO

NWMO has previously assessed the effects of temperature on the hydro-mechanical-chemical (HMC) properties of Wyoming sodium-dominant bentonite (e.g., MX-80); however, the specific effect of temperature-induced stress relaxation (creep) of bentonite swelling pressure has not been explicitly evaluated. As part of the collaboration group, NWMO plans to develop a scope of work to conduct coupled thermo–hydro–mechanical (THM) numerical modelling of the temperature-dependent creep behavior of bentonite swelling pressure under constant volume conditions. More details is given in Sec. 3.2.3.

3 Detailed research plan

3.1 Laboratory testing

Experimental work is planned by research teams of Charles University and SKB only. The planned experiments are summarised in **Table 4**.

Table 4: Planned experiments

Label:	**ALREADY DONE**
	TO BE DONE IN RELABEN
Experiment type	**BCV**
BENCHMARK: thermal relaxation, 1.6 g/cm3, 30days, 150°C, BCV only	CU (done), SKB
Thermal relaxation + cooling stress reduction – temperature effect (50, 75, 100, 125, 150), 1.6 g/cm3, 30days	CU (done), SKB (50°C and 100°C only)
Thermal relaxation + cooling stress reduction – dry density effect (1. 4, 1.6, 1.8 g/cm3), 150°C, 30days	CU (done), SKB (1. 4 and 1.8 g/cm3 only)
Thermal relaxation + cooling stress reduction – longer timeframe (90 days, or until stabilisation?) 1.6 g/cm3, 150°C	CU, SKB
Oedometric saturated creep – temperature effect (50, 75, 100, 125, 150°C), 1.6 g/cm3 (init.), 1.5 MPa	CU
Oedometric saturated creep – load effect (0.1, 1.5, 5 MPa), 1.6 g/cm3 (init.), 150°C	CU
Thermal cyclic (Equivalent to T72 test)	CU (done)

The experimental programme at Charles University will be carried out using T-MPC oedometers (**Figure 45**). The components exposed to high temperatures are made of invar to minimize the thermal expansion of the material. The samples will be compacted from 36 grams of BCV bentonite powder, which has an initial water content of 11%, directly into the test cells. The target dry density is 1.6 g/cm^3 and the target initial dimensions are d = 50 mm and h = 10 mm.

The test procedure is planned as follows. After sample preparation, the cell is be placed in the loading frame and a vertical stress of 1 MPa is applied via the lever arm. Deformation of the sample is monitored until full stabilization. After full equilibration, the sample is saturated from the bottom base under a low water pressure of 10 kPa. This generates partial swelling of the bentonite. When the swelling fully stabilizes, which is assumed to correspond to full saturation of the sample, both the top and bottom drainage systems are flushed. Back pressure of 500 kPa is then applied through the pressure controller. Back pressure application reduces effective stress, which leads to swelling. When sample height stabilizes, temperature is increased to its target value. The sample is then left at the elevated temperature for 12-24 hours to allow full temperature equilibration. After this, the sample is loaded with an additional 1 MPa (giving a total applied vertical stress of 2 MPa and effective vertical stress of 1.5 MPa). The sample is kept under constant conditions (no change in vertical stress, back pressure and temperature) for 30 days, with continuous monitoring of vertical deformation.

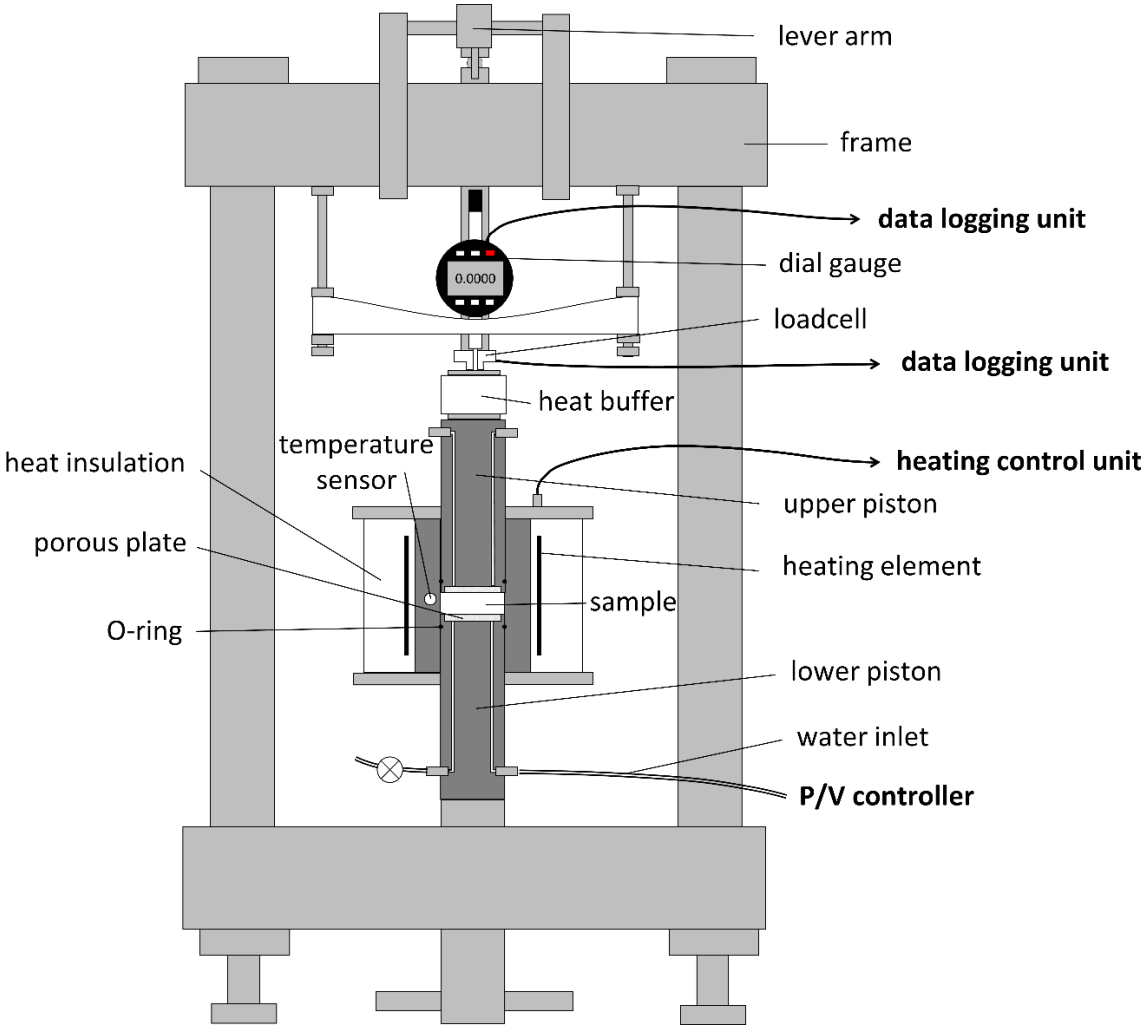

Figure 45: Configuration of the T-MPC oedometer during sample saturation (invar components are shown in dark grey; steel components are shown in light grey).

3.2 Modelling

3.2.1 Charles University (SURAO)

Modelling at Charles University will focus on further development of the VIBE constitutive model (Mašín, 2025). VIBE model (Viscohypoplastic bentonite model) is a coupled thermo-hydro-mechanical model for bentonite including double structure and rheological concepts. The model has been developed and validated with the experimental data available before the start of the RELABEN project (see Sec. 2.1). The following steps are planned to be done within RELABEN:

- Full validation of rheological models must include both relaxation and creep tests, as they are complementary (based on the same physical principles, investigated under different boundary conditions). Creep tests have, in addition, a significant advantage with respect to relaxation tests, as they are less sensitive to possible thermal mechanical response of the apparatus material. Within RELABEN, it is planned to involve the newly performed creep tests in the model validation. Potentially, if the results are not successful and both creep and relaxation tests cannot be simulated with the same set of material parameters, model formulation will be updated for the model to better reflect the observed behaviour.

- VIBE model has already been implemented within finite element codes SIFEL and Open-Geo-Sys. However, the effect of bentonite rheology has not yet been studied in simulation of full Mock-up tests, such as the Mock-Up Josef experiment or the EB200C experiment performed at Joseph underground laboratory. Within the RELABEN project, simulations of these experiments performed within different projects will be repeated with and without rheology to identify the effect of rheology within the timescale of the Mock-Up tests. This item may be studied with the initial version of the VIBE model, so that it is not necessary to wait for the new experimental data on bentonite creep performed within RELABEN. Once the new data (and, possibly, updated model) becomes available, the simulations will be repeated with the new model.

- A goal in studying the rheological effects is to investigate the response of the buffer material over the timespan of the repository. Simulations of the Mock-Up tests will be extended over the repository timespan, with realistic evolution of canister temperature to consider heating as well as slow subsequent cooling of the canister (within 100 to 10,000 years). These simulations will not target the effect of time only, but also the effect of cooling on swelling pressure decrease after the heating period. The final simulation time will be 1,000,000 years, in accordance with current guidelines for repository lifetime. While the simulations will only be valid to the limits of constitutive model and laboratory experiments based on which the model has been developed, they will provide a valuable insight into the repository behaviour not studied in simulations performed to data.

3.2.2 SKB

SKB will use a creep model that has been earlier developed in (Börgesson and Hernelind, 2006). This model has been implemented in COMSOL but can currently only be used with an elastic model. To get the initial stress state to use as an initial condition in the creep model an elasto-plastic THM model will probably be needed. The following steps are planned to be done within RELABEN:

- Modelling creep with the existing model to see if the behavior of reducing swelling pressure after heating could be explained by the creep model. Initially a THM model will

be used to find the initial condition and after that the creep model will be used to evaluate the change in axial swelling pressure with time during the relaxation period.

- As the water in the sample gets heated it will expand, this will cause an extra axial pressure. As the bentonite has a very low hydraulic conductivity it will takes some time for the water to exit the sample. This system will be modelled to evaluate if this process could cause the reduction in swelling pressure. Therefore, the intention is to model the effect of the expanding water due to the heating and how this water pressure dissipates out from the bentonite. This could be done by a TH model or if needed with a THM model.

3.2.3 NWMO

As part of the collaboration group, NWMO plans to develop a scope of work to conduct coupled thermo–hydro–mechanical (THM) numerical modelling of the temperature-dependent creep behavior of bentonite swelling pressure under constant volume conditions. This work will involve the development, calibration, and validation of a coupled THM numerical model, building on laboratory swelling pressure tests conducted, or to be conducted, at elevated temperatures that demonstrate accelerated pressure development followed by time-dependent stress relaxation.

The modelling will not explicitly represent microstructural processes within the bentonite (i.e., viscoplastic deformation and microstructural rearrangement) but will reproduce the observed stress relaxation at the macroscopic scale using a temperature dependent, time dependent constitutive formulation.

Model performance will be evaluated through comparison with measured laboratory test data, including swelling pressure evolution, peak values, and long-term relaxed pressures, supported by sensitivity analyses to assess the influence of temperature and key material parameters. The validated model will be applied to repository relevant thermal scenarios to improve confidence in long-term buffer performance predictions at elevated temperatures and to support design and safety assessment activities.

4 References

1. Mašín, D. (2025). Viscohypoplastic Bentonite (VIBE) Model. (submitted, preprint available at https://papers.ssrn.com/sol3/papers.cfm?abstract_id=5348185).

2. Najser, J. and Mašín, D. (2024). An experimental study on thermal relaxation of BCV bentonite. Applied Clay Science 254, 15 June 2024, 107374.

3. Villar, M. V., Cernochova, K., Cuevas, J., Gens, A., Gimeno, N., Graham, C., Harrington, J., Kaspar, V., Kaufhold, S., Leupin, O., Mašín, D., Najser, J., Olin, M., Reijonen, H., Šachlová, Š., Sayenko, S., Svensson, D., Svoboda, J., Vettese, G., Yliharju, J. and Zlobenko, B. (2025). State of the art on thermo-hydro-mechanical behaviour of clay buffers at high temperature. Frontiers in Nuclear Engineering 4.

4. Department for Business, Energy and Industrial Strategy, 2018, Implementing Geological Disposal – Working with Communities

5. Welsh Government, 2019, Geological Disposal of Higher Activity Radioactive Waste: Working with Communities.

6. Radioactive Waste Management, 2017, Geological Disposal Concept Status Report, NDA Report no. NDA/RWM/155.

7. Sellin, P., Leupin, O.X., 2013. The Use of Clay as an Engineered Barrier in Radioactive Waste Management: A review, *Clays and Clay Minerals*, **61**, 477-498

8. Daniels, K.A., Harrington, J.F., Zihms, S.G., Wiseall, A.C., 2017, Bentonite Permeability at Elevated Temperature, Geosciences, **7**, 3.

9. Graham, C.C., Daniels, K.A., Harrington, J.F., Chaaya, R. et al. 2024. Influence of Temperature on Clay Based Material Behaviour, EU

10. Birgersson, M., Karnland, O. och Nilsson, U., 2010. Freezing of bentonite: Experimental studies and theoretical considerations. SKB TR-10-40. Svensk kärnbränslehantering AB.

11. Karnland O, Olsson S, Nilsson U, 2006. Mineralogy and sealing properties of various bentonites and smectite-rich clay material. SKB TR-06-30, Svensk Kärnbränslehantering AB.

12. Karnland, O. Olsson, S. Dueck, A. Birgersson, M. Nilsson, U. Hernan-Håkansson, T. Pedersen, K. Nilsson, S. Eriksen, T.E. and Rosborg, B., 2009a. Long term test of buffer material at the Äspö Hard Rock Laboratory Final report on the A2 test parcel. SKB TR-09-29, SKB, Stockholm, Sweden.

13. Karnland O, Olsson S, Sandén T, Fälth B, 2009b. Long Term Test of Buffer Material at the Äspö HRL (LOT project) – Final report on the A0 test parcel. SKB TR-09-31, Svensk Kärnbränslehantering AB.

14. Olsson S, Karnland O, 2009. Characterisation of bentonites from Kutch, India, and Milos, Greece some candidate tunnel backfill materials. SKB R-09-53, Svensk Kärnbränslehantering AB.

15. Olsson S, Jensen V, Johannesson L-E, Hansen E, Karnland O, Kumpulainen S, Kiviranta L, Svensson D, Hansen S, Lindén J, 2013. Prototype Repository. Hydro-mechanical, chemical and mineralogical characterization of the buffer and backfill material from the

outer section of the Prototype repository. SKB TR-13-21, Svensk Kärnbränslehantering AB.

16. Svensson D, Dueck A, Nilsson U, Sandén T, Lydmark S, Jägerwall S, Pedersen K, Hansen S, 2011. Alternative buffer material. Status of ongoing laboratory investigation of reference material and test package 1. SKB TR 11 06, Svensk Kärnbränslehantering AB.

17. Svensson D, Bladström T, Sandén T, Dueck A, Nilsson U, Jensen V, 2023. Alternative Buffer Material (ABM) experiment. Investigations of test packages ABM2 and ABM5. SKB TR-23-25, Svensk Kärnbränslehantering AB.

18. Svensson D, Bladström T, Dueck A, Nilsson U, Jensen V, Lindén J, Lindroos F, Turner S, Hillier S, 2024. Long term test of bentonite buffer (LOT) at the Äspö HRL. Evaluating bentonite stability in the LOT A3 and S2 experiments after 20 years of heating. SKB TR-24-02, Svensk Kärnbränslehantering AB.

19. Börgesson L and Hernelind J, 2006. Canister displacement in KBS-3V. A theoretical study. SKB TR-06-04. Svensk kärnbränslehantering AB.

www.igdtp.eu // secretariat@igdtp.eu